

Diffusive turbulence in a confined jet experiment

By FRÉDÉRIC RISSO AND JEAN FABRE

Institut de Mécanique des Fluides de Toulouse, Allée du Professeur Camille Soula,
31400 Toulouse, France

(Received 19 June 1995 and in revised form 4 December 1996)

An experimental analysis of the turbulence in an axisymmetrical jet within a closed tube is presented. At some distance from the nozzle, a turbulent region develops, where the kinetic energy of the mean flow almost vanishes. In this region, the turbulence is transported by turbulent diffusion and its energy decreases with the distance from the inlet. A complete description of the flow field has been achieved using laser Doppler anemometry. Some unusual features are highlighted: the statistical moments of the velocity decay exponentially, the integral length scales remain constant, the radial profiles are self-similar and the Reynolds stress tensor is isotropic and homogeneous in the radial direction. These results highlight the roles of pressure fluctuations and any mean residual motion in the return to isotropy.

1. Introduction

To understand the fundamental properties of turbulence, investigating the ideal situations where the contribution of mean motion is negligible is particularly useful. The simplest case was selected by Batchelor (1953) to build his famous theory of homogeneous and isotropic turbulence. In this case, however, the turbulent transport due to the triple velocity correlations vanishes. As these terms are poorly understood, several authors have focused their attention on inhomogeneous turbulence without mean velocity gradient. Veeravalli & Warhaft (1989) performed an experimental investigation of a ‘shearless turbulence layer’, created by matching two decaying grid turbulences with different length scales and an identical mean velocity. They found that, when gradients of mean flow are negligible, the turbulent transport is related to intermittence and non-Gaussianity. Such a situation where turbulent transport dominates has received particular interest with a view to improving the turbulence models. Sonin (1983) used an analytical solution of the k - ϵ model in the case of purely diffusive turbulence to find a relation between the constants of the model. Lele (1985) found another relation for the diffusion of turbulence in a quiescent fluid. More recently, Magnaudet (1993) used available data from diffusive turbulence to develop a second-order closure model.

Surprisingly, most of the experiments devoted to inhomogeneous turbulence in the absence of mean flow have been conducted without the main objective of improving our fundamental knowledge of turbulence. Indeed, the literature contains several examples of turbulent fields without mean motion realized for specific purposes. From a historical point of view, the first experiment was carried out to investigate the interaction of turbulence with a density layer (Rouse & Dodu 1955; Turner 1968). The second was initiated by Sonin, Shimko & Chun (1986) to study the role of turbulence on vapour condensation at a free surface. The third was to study the

deformation experienced by a bubble in a turbulent field (Risso 1994). In both the first and the second experiments, the objective was similar: the mean flow had to be cancelled in order for the mixing near the interface to be controlled by turbulence only. In the last experiment, it was necessary to suppress the mean flow to increase the residence time of a bubble within the turbulent test section so that a possible secondary contribution to the bubble deformations could be eliminated.

Unfortunately, there is no way, at least experimentally, to obtain the ideal situation of homogeneous, isotropic and stationary turbulence with zero mean velocity. Indeed, the turbulent energy is dissipated at smallest scales by viscous forces. The loss of energy has to be compensated by supplying, at a certain time or location, energy at the largest scales. This production of turbulent energy is done by the work of turbulent stress through the mean rate of strain. Thus, turbulence cannot exist if a mean flow never and nowhere existed. However, this ideal situation can be approached. A first solution consists of producing the turbulence by an intense mixing. After the mean flow has been suppressed, an homogeneous and isotropic turbulence that decays with time can be obtained. Practical solutions have tended to use spatially decaying turbulence obtained by the passage of a uniform flow across a grid (Batchelor & Townsend 1947; Stewart & Townsend 1951; Corrsin 1963; Uberoi 1963; Comte-Bellot & Corrsin 1971). Even when this solution produces quasi-isotropic stationary turbulence, it implies the presence of an important mean advection which cannot be accepted in the three aforementioned situations. Another solution leads to stationary flow without advection but the homogeneity in one direction is lost. Turbulence is produced by a steady flow and transported by turbulent diffusion far from the region where it was created. This is 'diffusive turbulence' which transports itself and decays as it moves from the production region. In the present study, we shall focus on the properties of the turbulence that diffuses by eddy motion in the z -direction and possesses homogeneity only in the perpendicular plane xOy . Is this situation possible?

It is easy to show that the strict answer is no. Indeed, what does homogeneity and isotropy sustain and induce? It is well known that these properties imply invariance through translation and rotation of the different moments involving velocity components or pressure of the fluctuating field. As a consequence of homogeneity with respect to the direction x_i , the spatial derivatives, $\partial(\cdot)/\partial x_i$, must be identically equal to zero. Moreover, a necessary – but not sufficient – condition of isotropy is that the Reynolds stress tensor must be spherical. Let us consider a turbulent field without mean motion, homogeneous with respect to both x and y , that diffuses in the z -direction. The transport equations of the Reynolds stress tensor become (see the Appendix, equation (A1)):

$$-\frac{\partial}{\partial z} \overline{u_z u_x^2} + \frac{2}{\rho} \overline{p \frac{\partial u_x}{\partial x}} + 2\epsilon_x = 0, \quad (1)$$

$$-\frac{\partial}{\partial z} \overline{u_z u_y^2} + \frac{2}{\rho} \overline{p \frac{\partial u_y}{\partial y}} + 2\epsilon_y = 0, \quad (2)$$

$$-\frac{\partial}{\partial z} \overline{u_z u_z^2} - \frac{2}{\rho} \frac{\partial}{\partial z} \overline{p u_z} + \frac{2}{\rho} \overline{p \frac{\partial u_z}{\partial z}} + 2\epsilon_z = 0, \quad (3)$$

$$-\frac{\partial}{\partial z} \overline{u_z e} - \frac{2}{\rho} \frac{\partial}{\partial z} \overline{p u_z} + 2\epsilon = 0, \quad (4)$$

where u and p are the velocity and pressure fluctuations, ρ the density, e the instan-

taneous square-velocity, ϵ the turbulent dissipation rate and the overbar denotes a statistical or time average. For the turbulence to diffuse, there can be no homogeneity with respect to z . In addition, the isotropy cannot be strictly achieved. Indeed, if the turbulence is isotropic, all the terms of (1) to (4) except for the dissipation term must cancel. As the triple correlations are related to the spatial transport of turbulent energy by turbulent diffusion, it is not surprising that the lack of homogeneity leads to a restriction on isotropy. However, there is some hope that the tensor of the second-order moments, i.e. the Reynolds stress tensor, is isotropic even if the tensor of the third-order moments is not. Indeed, when the production by the mean flow vanishes, one would expect the turbulence to approach a state in which turbulent energy is distributed equally in each direction. To avoid any confusion, this weak isotropy will be further referred to below as ‘energetic isotropy’.

Nevertheless, the analysis of (1) to (4) shows that there is no obvious reason why energetic isotropy occurs in such a flow. Let us assume that the Reynolds stress tensor is spherical in a given plane $z = z_0$. It is likely that the correlation between z -fluctuations and z -energy $u_z u_z^2$ is greater than that between z -fluctuations and x -energy $\overline{u_z u_x^2}$. For isotropy to continue to be preserved, say at $z = z_1 > z_0$, another mechanism is needed to compensate for this imbalance. If we accept that the dissipation, which involves the smallest-scale eddies, is isotropic, only the pressure–velocity correlation can take this role. When turbulence production is negligible, Magnaudet (1993) found, for nearly homogeneous and isotropic turbulence, that $\partial u_z u_x^2 / \partial z = \partial(u_z u_z^2 + (2/\rho)\overline{p u_z}) / \partial z = -\frac{2}{3}\epsilon$ and that $\overline{u_z^3}$ is three times $u_z u_x^2$. Thus, the condition for the energetic isotropy to be maintained becomes $\overline{p u_z} = -\rho \epsilon \overline{u_z} / 5$. According to this, the diffusion by pressure fluctuations should balance the relative excess of diffusion by z -velocity fluctuations for energetic isotropy. However, we are still unable to predict the behaviour of the diffusive turbulence from theoretical grounds. What does an experiment tell us about it?

To the best of our knowledge, only two different kinds of experimental set-ups have been used to produce diffusive turbulence. The first was done by Rouse & Dodu (1955), followed by Bouvard & Dumas (1967) and Turner (1968). Many subsequent experiments used a similar arrangement, namely Thompson & Turner (1975), Hopfinger & Toly (1976), McDougall (1979), Brumley & Jirka (1987), Hannoun, Fernando & List (1988), De Silva & Fernando (1992) and Fernando & De Silva (1993). The turbulence is produced by a horizontal grid oscillating in the vertical direction inside a square tank. At a certain distance, z , far from the grid, diffusive turbulence whose kinetic energy decays as z^{-2} and whose integral length scales increase linearly with z is obtained. A residual mean flow has been often observed, such as that pointed out by Hopfinger & Toly (1976). In his experiment, McDougall (1979) tried to analyse its structure but the phenomenon was too complex to interpret. More recently, Fernando & De Silva (1993) claimed that the mean flow may be eliminated by a judicious choice of the near-wall shape of the grid. In addition to the residual mean flow, energetic isotropy is never realized in any of these experiments. In the best case, the ratio between horizontal and vertical r.m.s. velocities is equal to 1.2. Because this flow condition was considered more as a tool than as a subject of investigation, none of the foregoing studies presented a whole description of the flow field. There are, however, some interesting conclusions worth quoting. Hopfinger & Toly (1976) have used (4) and assumed that all statistical moments involved are proportional to $\overline{u_z^2}^{3/2}$. The measurements of Hanoun *et al.* (1988) show that $\overline{e u_z} = 2\overline{u_z^3}$.

In the experiments of Sonin *et al.* (1986), the turbulence is produced differently. The

experiment consisted of an axisymmetric jet discharging through a nozzle into one end of a tube. The tube is closed at its other end so that the fluid must be evacuated through an orifice near the nozzle. At a certain distance from the nozzle, the mean motion decreases sufficiently for diffusive turbulence to develop. In this region, the turbulent kinetic energy decays exponentially and the integral length scales remain constant. Despite these promising results, a detailed investigation of the turbulence properties has not yet been carried out.

The goal of this paper is to fill this gap, with the aim of improving our understanding of the mechanisms involved in flows dominated by turbulent transport. The confined jet experiment was chosen here for several reasons. This configuration guarantees stationary boundary conditions whereas the oscillating grid may lead to periodic fluctuations of the velocity field interacting with the turbulent motion. The geometry is simple and enables a complete investigation of the flow field.

2. Experimental set-up and instrumentation

The test section consisted of a glass tube of inside diameter, $D = 77$ mm, and length $H = 600$ mm. The tube is closed at the top (figure 1). Both the inlet and outlet for the liquid are located at the bottom. The liquid enters through a circular nozzle of diameter $d = 10$ mm, centred at the axis. It is evacuated through an annular passage having an inner diameter $D' = 70$ mm, and an outer diameter D . Special care was taken to guarantee the symmetry of both nozzle and annulus with respect to the tube axis. The liquid is supplied from a centrifugal pump to the nozzle through a convergent section. This ensures a uniform velocity profile and a turbulence intensity of less than 2% at the inlet of the test section. Tap water was used for the present experiments with velocity at the nozzle exit, U_0 , in the range 2–10 m s⁻¹. Before each experiment, this velocity was measured at the axis and its stability with time was carefully checked.

Most of the experimental results were obtained in the aforementioned geometry which will be referred further to as 'test section 1'. However, to check the sensitivity to the flow geometry, a two-thirds-scaled test section with variable length, referred to as test section 2, was used. The flow conditions are characterized by the four dimensionless numbers: the Reynolds number, $Re = U_0 D / \nu$, the nozzle-to-tube diameter ratio, $\alpha = d/D$, the inlet to outlet area cross-section ratio, $\beta = d^2/(D^2 - D'^2)$, the diameter-to-length ratio, $\gamma = H/D$.

The experiments were carried out for the following flow conditions: for test section 1 $\alpha = 0.195$, $\beta = 0.22$, $\gamma = 7.7$, $Re = 150\,000$; for test section 2, $\alpha = 0.186$, $\beta = 0.22$, $\gamma = 6.7, 8.1, 9.6$, $Re = 20\,000, 45\,000$ and $95\,000$.

The instantaneous velocity was measured by laser Doppler anemometry (LDA). Two kinds of measurements were done. On the one hand, simultaneous one-point measurements of either axial and azimuthal or axial and radial velocity components were performed. The correlations between the velocity components could be determined except for the cross-correlations involving radial and azimuthal components. On the other hand, simultaneous two-point measurements of the axial velocity component were made. One point was fixed on the axis while the coordinates of the other point were varied, either in the axial or radial direction.

Two sets of LDA equipment were used. The main one consisted of an argon Spectra Physics 2 W laser and a Dantec Fiber Flow anemometer with a two-dimensional optical probe of 60 mm. It was used with a Bragg cell, a beam expander and a 310 mm lens, in backward scattering mode for the one-point measurements.

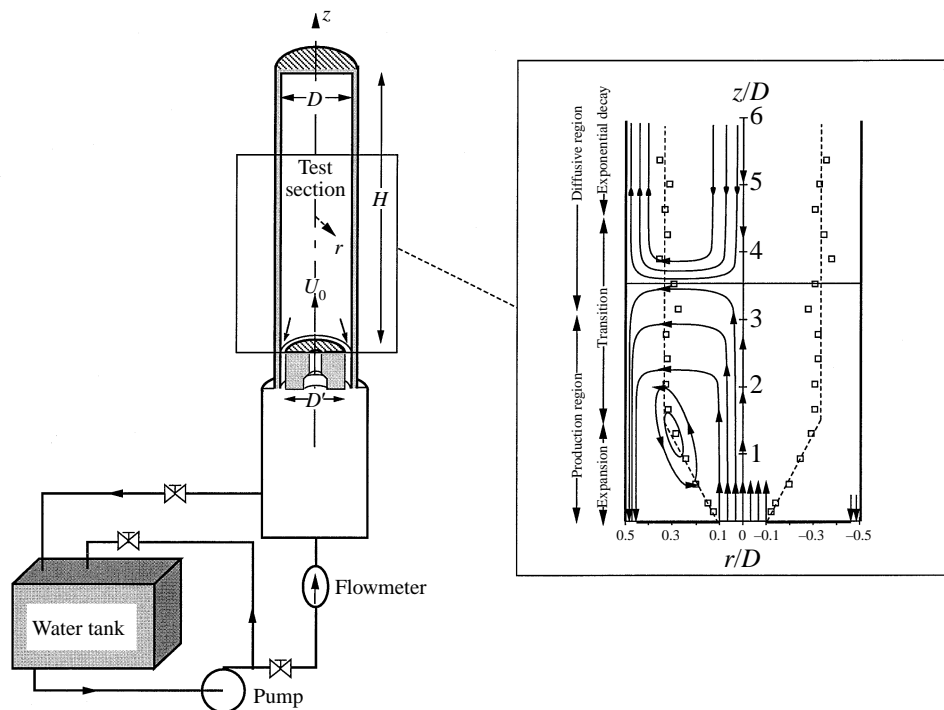


FIGURE 1. Experimental apparatus and the qualitative mean velocity field: points where $U_z = 0$.

Additional equipment, including a helium–neon Spectra Physics 35 mW laser and a 55X modular optics with a focal length of 300 mm, was used for the two-point measurements. This less-powerful LDA was used in forward-scattering mode. It was kept fixed while the optical probe of the main equipment was shifted to different axial or radial locations.

The optical probe was fixed vertically on a gear which could be displaced horizontally in two perpendicular directions. The laser source and the photomultiplier of the additional equipment were kept fixed together on another gear that could be displaced vertically. The displacement of the measuring volume was obtained with an uncertainty of $\pm 1/10$ mm.

The Doppler signals were processed with Dantec Burst Spectrum Analysers, model 57N10. The data were recorded on the hard disk of a personal computer and ultimately processed with custom software. The results from the digital signal processing were compared to the output of two analog voltmeters for mean and r.m.s. values respectively. The independence of the measurements with respect to the magnitude of the Bragg shift was also verified. A water-filled transparent Plexiglas box with parallel sides was placed around the cylindrical tube to reduce the optical refraction through the wall of the tube. The residual optical refraction of the laser beam induced small errors in the measurements of the radial and azimuthal components of the velocity. These errors never exceeded 1.5% of the magnitude of the velocity and 3.5° for its direction. They were corrected, in both position and magnitude, with custom software.

Mean velocity, various velocity moments up to fourth-order, time correlation functions and frequency spectra were determined from the one-point measurements whereas space correlation functions were determined from the two-point measure-

ments. The statistical moments of the velocity $\overline{u_i^m(\mathbf{x}, t)}$ were determined from statistical averages, each sample being weighted by the interval between its arrival time and that of the preceding sample. The time for data acquisition was between 200 and 1000 s. This allowed 10^4 to 10^5 samples to be used for the determination of the statistical averages. In each case, this number was large enough to ensure that the statistical convergence was better than 1% for the mean velocities and standard deviations, and better than 3% for the third and fourth moments. Besides, the results were reproducible. The differences at locations where the measurements were the most error-prone never exceeded 4% for the mean velocity and standard deviation, and 8% for the third and fourth moments.

The symmetry of the flow with respect to the axis was carefully checked by using different tests. It was verified from the profiles of the three velocity components over the pipe radius. The verification was done for $\theta = 0$ and $\theta = \pi$ at six different longitudinal cross-sections and for $\theta = \pi/2$ and $\theta = 3\pi/2$ at three of them. Up to the fourth-order moments, the symmetry was clearly observed (see for example figure 9 where the radial profiles of the mean velocity and standard deviation of two components of the velocity were plotted for $\theta = 0$ and $\theta = \pi$). For standard deviations, the errors found were always less than 3%. Furthermore, the mean θ -component magnitude was always negligible (less than 1% the axial one). There was no swirl. Finally, the mean r -component and the turbulent shear stress measured on the axis of symmetry were negligible in comparison with the mean and the standard deviation of the axial velocity respectively (less than 1%).

The conservation of mass was checked by integration of the radial profiles of the axial mean velocity which must be zero. The maximum error was everywhere less than 4% of the inlet flow rate. Because pressure could not be measured within the tube, the conservation of mean momentum was not checked.

The determination of the one-point or two-point cross-correlations $\overline{u_i^m(\mathbf{x}, t)u_j^n(\mathbf{x} + \boldsymbol{\xi}, t)}$ was also obtained from statistical averages of products involving two velocity components. However, since each component was randomly sampled by the LDA, the simultaneity of each pair of samples was not ensured. A criterion which retains the pair of velocity samples falling within a given time interval Δt , was applied. For the one-point correlations, Δt was taken to be equal to 0.01 ms, and for the two-point correlations 1 ms for $z/D = 3.9, 4.5$ and 2 ms for $z/D = 5.2$. The time-velocity correlation functions $\overline{u_i^m(\mathbf{x}, t)u_j^n(\mathbf{x}, t + \tau)}$ were determined with a similar method. The statistical averages at each time lag $\tau = n\Delta\tau$ were calculated over all the pairs of velocity components that fall within the interval $[(n - 0.5)\Delta\tau, (n + 0.5)\Delta\tau]$. The frequency spectra were determined with an FFT algorithm from blocks of 2048 velocity data points that were numerically resampled at a constant rate from the original data using an interpolation algorithm.

3. General description of the flow field

3.1. Evolution of mean velocity and turbulence on the axis

The turbulent flow of a jet in a closed tube has some original features which can be highlighted, using the evolution of the mean velocity and higher moments on the tube axis. The coordinates will be scaled by the tube diameter, D . This choice is dictated by a reason that will be clarified below. The longitudinal component of the mean velocity U_z , scaled by the velocity at the inlet U_0 , is plotted versus the distance from the inlet z in figure 2. Over a short distance of about $0.5D$ the velocity remains constant as in the

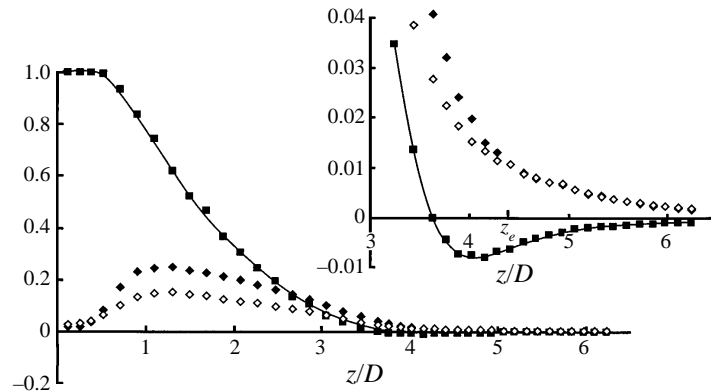


FIGURE 2. Mean and r.m.s. velocities on the axis: ■, U_z/U_0 ; ◆, $\overline{u_z^2}/U_0$; ◇, $\overline{u_r^2}/U_0$.

potential core of a free jet. Then the velocity decreases strongly under the influences of both turbulent diffusion and flow confinement. Turbulent diffusion is responsible for the transfer of momentum from the axis to the surrounding fluid similar to a free turbulent jet. However, in contrast to the unbounded case in which the total flux of momentum remains nearly constant with the distance, for the present geometry, the total flux of mass must remain constant with z . The mixing process causes the velocity profile to flatten with z and the total flux of momentum to decrease. This decay can only be compensated by an adverse pressure gradient which, in turn, makes the velocity drop faster with z . Nevertheless, instead of approaching zero asymptotically, the mean velocity cancels near $z = 3.6D$. It continues to decrease further through negative values. The velocity reaches a minimum value for $z = 4.3D$ from which it increases slowly to zero.

The general evolution of the turbulent quantities with respect to z is less surprising. Figure 2 displays the standard deviation of the longitudinal and radial components $\overline{u_z^2}^{1/2}$, $\overline{u_r^2}^{1/2}$ of the velocity. In the potential core, the velocity gradients are negligible and the turbulence level is weak. The fluctuations are induced by the growing mixing layer and increase roughly by the square of the distance from the jet exit (Sunyach & Mathieu 1969). Farther away than $z \approx D$, owing to the high-strain-rate turbulence, production leads to intense non-isotropic turbulence at the jet boundary. As in unbounded jets, the standard deviations decrease with z due to the diminution of the velocity gradient. The turbulence energy is redistributed from the axial component to the other components, so that $\overline{u_z^2}^{1/2}$, and $\overline{u_r^2}^{1/2}$ become nearly equal at some distance from the inlet. We shall see later that the flow reaches an asymptotic state at this particular location $z_e = 4.4D$.

As expected, the turbulence decay is less rapid than that of the mean flow. This can be seen in figure 3 in which the ratio of the r.m.s. to the mean velocities $\overline{e}^{1/2}/U$ has been plotted. This ratio continuously increases from the inlet. It becomes infinite at the point where the mean velocity vanishes. It then decreases but remains between 300% and 500%. In this flow region the turbulence is significantly greater than the mean motion. In parallel, the axial-to-radial r.m.s. velocities ratio $(\overline{u_z^2}/\overline{u_r^2})^{1/2}$ (figure 3), which is initially about 1.7, decreases regularly and reaches unity at z_e . There is a tendency towards isotropy far enough from the inlet.

The evolution of some of the higher moments of the velocity are plotted in figure 4 versus the distance, except for the region near the jet core. The moment $\overline{u_z^3}$,

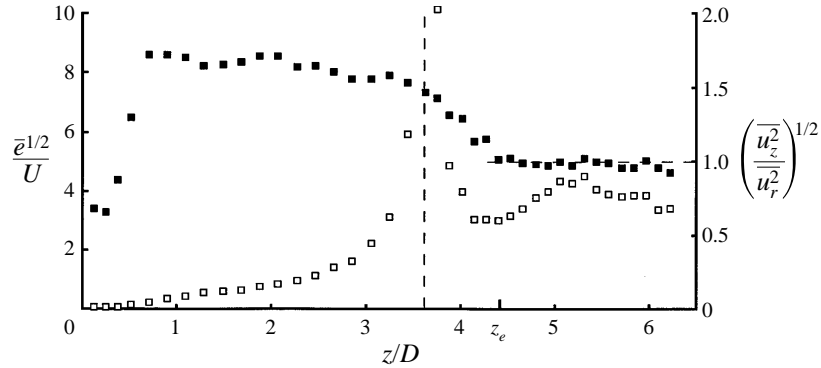


FIGURE 3. Relative intensity of turbulence on the axis: \square , $\bar{e}^{1/2}/U$. Isotropy ratio on the axis: \blacksquare , $(\bar{u}_z^2/\bar{u}_r^2)^{1/2}$.

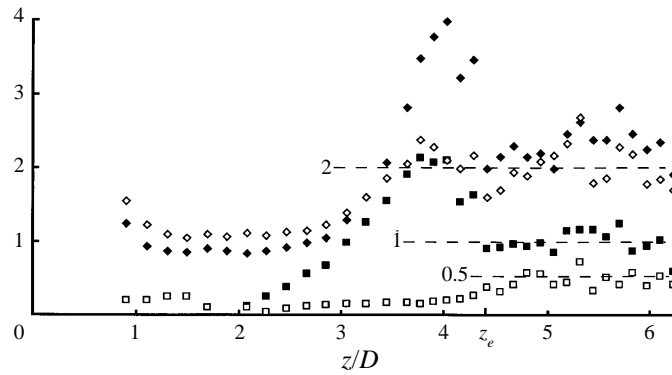


FIGURE 4. Ratio between statistical moments on the axis: \blacksquare , $\bar{u}_z^2/\bar{u}_z^{3/2}$; \square , $\bar{u}_z \bar{u}_r^2/\bar{u}_z^3$; \blacklozenge , $\frac{1}{3} \bar{u}_z^4/\bar{u}_z^2$; \diamond , $\frac{1}{3} \bar{u}_r^4/\bar{u}_r^2$.

responsible for the diffusion of the z -velocity fluctuations, is normalized by $\bar{u}_z^{3/2}$. This ratio introduces the skewness factor of the z -component. It increases from zero near $z = 2D$ to reach its maximum at $z \approx 3.9D$, then decreases and reaches unity from $z = z_e$. The third-order moment, $\bar{u}_z \bar{u}_r^2$, responsible for the diffusion of the r -velocity fluctuations is normalized by \bar{u}_z^3 . This ratio always remains smaller than unity and increases to reach a constant value of 0.5. The fourth-order moments, \bar{u}_z^4 and \bar{u}_r^4 , are normalized by \bar{u}_z^2 and \bar{u}_r^2 respectively. The corresponding ratios introduce the flatness factors of the axial and radial velocity fluctuations. They both approach a value nearly equal to 6 from $z > z_e$. From these results, it may be noted that the turbulence is close to Gaussianity only in the very short region $1.5 \leq z/D \leq 2.3$. In this region, the inlet conditions are forgotten and the diffusion of turbulence is not yet predominant so that turbulence is controlled by the mean velocity gradient. Elsewhere, the statistical behaviour of the turbulence is much more complex.

The evolution with respect to z of the double, triple and quadruple velocity correlations of u_z and u_r are shown in figure 5 using a semi-log representation. From z_e , the evolutions appear almost linear with $\ln(z)$. The n th order moment M_n decays exponentially with z as

$$M_n(z) = M_n(z_0) \exp[-(z - z_0)/L_n].$$

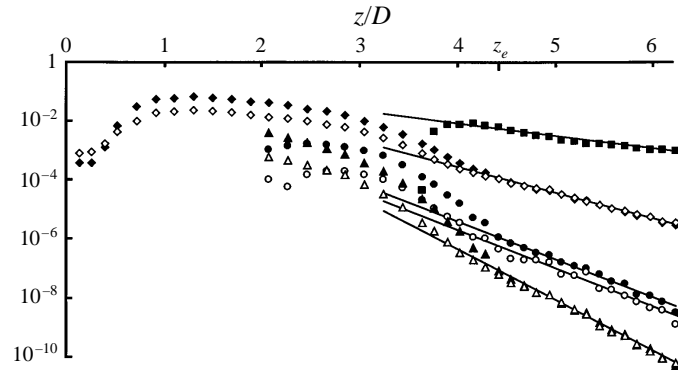


FIGURE 5. Statistical moments on the axis: ■, $|U_z|/U_0$; ◆, $\overline{u_z^2}/U_0^2$; ◇, $\overline{u_r^2}/U_0^2$; ●, $\overline{u_z^3}/U_0^3$; ○, $\overline{u_r^3}/U_0^3$; ▲, $\overline{u_z^4}/U_0^4$; △, $\overline{u_r^4}/U_0^4$.

	U_z	$\overline{u_z^2}$	$\overline{u_r^2}$	$\overline{u_z^3}$	$\overline{u_z u_r^2}$	$\overline{u_z^4}$	$\overline{u_r^4}$
L/D	0.96	1.00	1.01	1.03	1.03	1.02	1.02

TABLE 1. Exponential scales of decay

More interesting is the fact that the characteristic length scale of decay L_n of the n th-order moment is simply equal to L/n , where L is the same for all the moments. Thus $M_n^{1/n}$ follows the same law whatever the value of n . The law of decay is the same provided that each moment be expressed in the same dimension:

$$M_n(z) = M_n(z_0) \exp \left[-n \frac{z - z_0}{L} \right]. \quad (5)$$

The values of L were determined using a least square fit of (5) and are given in table 1. It turns out that this length scale is nearly equal to the tube diameter, $L = 1.0D$. Straight lines corresponding to (5) have been drawn on figure 5, showing the good agreement with the experimental results. Far from the inlet, the flow behaviour is controlled by the lateral confinement, thus confirming *a posteriori* the choice of the diameter for scaling the coordinates.

The kinematic structure of mean and turbulent properties of the velocity field on the tube axis shows some peculiarities of the flow behaviour. Indeed, both lateral confinement due to the tube wall and longitudinal confinement caused by the endwall, compel the flow to restructure from a typical shear flow ($0 \leq z \leq 1.5D$) to an exponentially decaying diffusive turbulence ($z \geq z_e$). The transition between these two states involves different successive steps. The first step takes place in the region dominated by the mean velocity. The interaction of the mean flow with the tube boundary causes the jet expansion to stop. This is illustrated in figure 1 by the behaviour of the line of zero axial velocity near $z = 1.5D$. The second step is more gradual. The mean velocity progressively decreases and the flow becomes dominated by the turbulence near $z = 3D$. As the turbulence level is not maintained by production, it decays with z and the size of the larger eddies increases. The third step is when their size reaches the tube diameter. They stop growing and the turbulent scale is controlled by the tube diameter.

The above physical distinction between different flow regions is reinforced by the

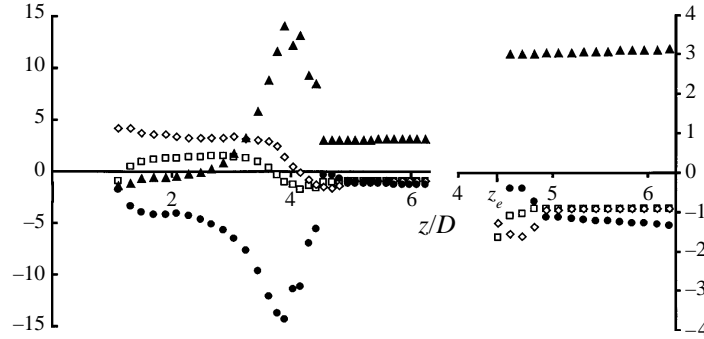


FIGURE 6. Budget on the axis of the second-order moments of turbulence: \square , Ad_z^* ; \diamond , $P_{i_z}^*$; \blacktriangle , Tu_{zz}^* ; \bullet , $Rest_z^*$ (the region $z > 4$ is shown on an expanded scale on the right).

analysis of the turbulent budget (see the equations and definitions in the Appendix). For this purpose the different terms involved in the transport equation of u_z^2 , i.e. the turbulent diffusion in the z -direction Tu_{zz}^* , the advection by the mean flow Ad_z^* and the production by the mean strain rate $P_{i_z}^*$, have been plotted in figure 6 at the tube axis. The radial turbulent diffusion Tu_{zr} , the dissipation \mathcal{E}_z^* and the two terms involving the pressure fluctuations $\mathcal{T}p_z$ and $\mathcal{R}p_z$ have been grouped together into the rest $Rest_z^*$ which has been determined from the difference. Note that the starred quantities are made dimensionless by dividing the non-starred quantities in (A2) by $\overline{u_z^2}^{3/2}/D$. In the whole region dominated by the mean flow ($z \leq 3D$), the turbulence is mainly controlled by a classical balance between production and dissipation. Farther away from the inlet, the contribution of the turbulent diffusion to the total budget increases and, for $z > 3D$, the turbulence is controlled by a diffusion–dissipation balance. However, beyond z_e , the turbulence decays exponentially and the relative contribution of each term in the turbulent budget remains constant. This particular turbulence will be analysed further in detail.

3.2. Sensitivity to the dimensionless parameters

We have first considered the results obtained in test section 1 at $Re = 150\,000$ and for a specific flow geometry, namely $\alpha = 0.195$, $\beta = 0.22$, $\gamma = 7.7$. We shall discuss now whether this structure is maintained when the Reynolds number and the flow geometry are changed. For this purpose, test section 2 was used. Basically, this test section has nearly the same nozzle-to-tube diameter ratio α (0.186) and the same inlet to outlet cross-section ratio β , but its length can be modified.

Apart from our experiments, only few other data sets exist in the literature, and the axisymmetric jet in a closed pipe has not been investigated in much detail. To our knowledge, the earlier experiments, mentioned in Abramovich (1963), are due to Rosenberg (1963). His results show the mean velocity of the axis of a jet issuing from an inner tube of diameter d , placed in an outer tube of diameter D . Two different outer tubes were utilized by Rosenberg. Using our notation, his experiments correspond to $\alpha = 0.186$, $\beta = 0.053$ and to $\alpha = 0.087$, $\beta = 0.0092$. Neither the Reynolds number nor the tube length were specified. More recent results have been obtained on the axisymmetric confined jet at MIT by Sonin *et al.* (1986), Brown, Khoo & Sonin (1990), and Khoo & Sonin (1992). Their pipe was closed by a plug at the bottom while the top was the liquid surface instead of a rigid wall. The inlet consisted of a tube, symmetrically placed through the plug, with the outlet tube located next to

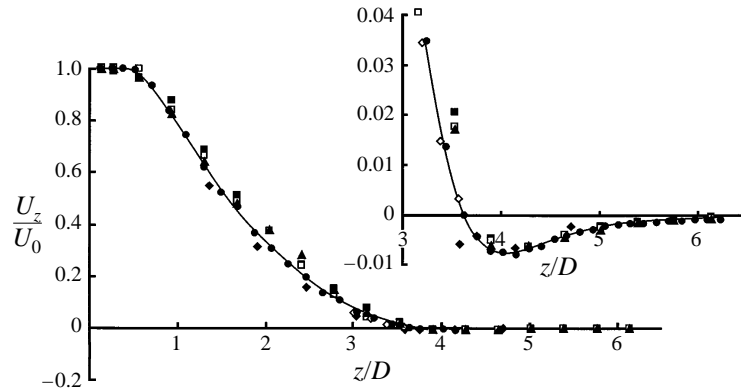


FIGURE 7. Mean velocity on the axis: U_z/U_0 . Test section 1: \bullet , $Re = 150\,000$, $\gamma = 7.7$. Test section 2: \blacksquare , $Re = 22\,000$, $\gamma = 6.7$; \square , $Re = 45\,000$, $\gamma = 6.7$; \diamond , $Re = 45\,000$, $\gamma = 8.1$; \blacklozenge , $Re = 45\,000$, $\gamma = 9.6$; \blacktriangle , $Re = 97\,500$, $\gamma = 6.7$.

the inlet tube. Near the outlet, the symmetry with respect to the axis is thus broken. With their geometry, the nozzle-to-tube diameter ratio is $\alpha = 0.05$ but β cannot be determined. They performed observations of solid tracers and measured the velocity field by LDA. Later, Khoo *et al.* (1992) used a PIV method in an identical facility.

Figure 7 shows the distribution of mean velocity on the tube axis for $Re = 22\,000$, $45\,000$, $97\,500$ and $150\,000$. In this range, since the flow is not sensitive to the Reynolds number, the results are identical. In particular, the coordinate at which the mean velocity vanishes is the same for each case. We have also verified that the r.m.s. velocities do not depend on the Reynolds number. This invariance property has been already demonstrated by Sonin *et al.* (1986) and Khoo & Sonin (1992) in the exponentially decaying region. They showed that no influence can be detected for $Re > 25\,000$. From a practical point of view, this behaviour is of major interest since the turbulence level can be chosen by adjusting the inlet velocity, without any significant consequences for the flow structure.

In studying the influence of the tube length, another interesting conclusion can be reached. Four different geometries have been used, characterized by the values of the diameter-to-length ratio $\gamma = 6.7, 7.7, 8.1, 9.6$. As shown in figure 7, the conclusion is the same as for the Reynolds number. No influence can be observed provided that the tube is long enough for the region of exponential decay to develop. Indeed, the evolution of the flow structure from the initial turbulence, dominated by production, to the final one, dominated by diffusion, though essentially related to the existence of the closed end, is independent of its location. Whether the tube is confined by a plug or by a free surface the results are identical, except near the end where the boundary conditions are not the same.

The inlet-to-outlet area cross-section ratio β also has a weak influence, acting mainly on the total pressure drop between the inlet and the outlet. In contrast to β , γ and Re , to which the flow structure is weakly sensitive, the nozzle-to-tube diameter ratio α is the key geometrical parameter because it characterizes the lateral confinement. This is clear for the mean velocity whose axis evolution is displayed on figure 8. Our results are compared to the results for a confined jet in a closed tube of Rosenberg (1963) and those of a free axisymmetrical jet in an unbounded medium of Chassaing (1979). For the result to be compared to the free jet case, the z -coordinate was normalized by the nozzle diameter d . For $\alpha = 0.186$, our results coincide with

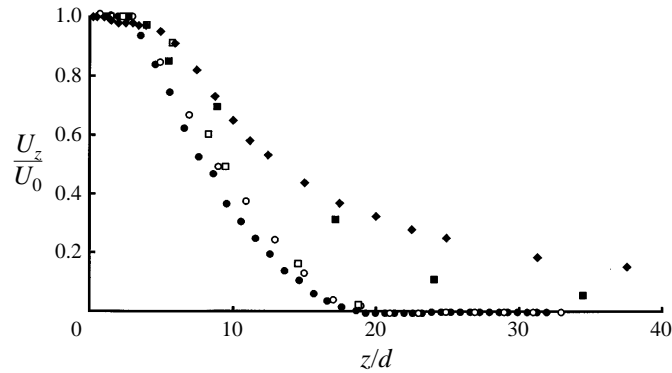


FIGURE 8. Mean velocity on the axis: U_z/U_0 . Test section 1: \bullet , $\alpha = 0.195$, $\beta = 0.22$. Test section 2: \circ , $\alpha = 0.186$, $\beta = 0.22$. Abramovich (1969): \square $\alpha = 0.186$, $\beta = 0.053$; \blacksquare , $\alpha = 0.087$, $\beta = 0.0092$. Chassaing (1979): \blacklozenge , $\alpha = 0$ (free jet).

those of Rosenberg. In the experiments of Sonin *et al.* (1986), Khoo & Sonin (1992) and Khoo *et al.* (1992) the value of α is 0.05. Unfortunately, they did not perform a complete investigation of the flow since they did not give the mean velocity. Although the results are far from extensive, we may, however conclude from figure 8 that the greater α becomes, the faster the decay of the mean velocity with respect to z . The influence of α on the turbulence, the flow structure and the properties of the diffusive region, does not clearly emerge from these results. Sonin *et al.* (1986), Khoo & Sonin (1992) and Khoo *et al.* (1992) determined the evolution of the r.m.s. velocity and of the diffusive time and length scales for $z > 3D$, from where the isotropy ratio $(\overline{u_z^2}/\overline{u_r^2})^{1/2}$ is nearly equal to unity in their geometry. Their results prove the existence of an exponentially decaying zone of turbulence. Its corresponding length scale L , as defined in (5), was found equal to $1.2D$ in the experiments of Sonin *et al.* (1986) whereas it was $0.74D$ in the experiments of Khoo *et al.* (1992) for the same flow conditions. They do not agree with our result since this length scale was found in our experiments to be $L = 1.0D$ (see table 1). According to this, the role of the key parameter α remains unclear. However, the existence of a diffusive exponential zone is shown to exist for α in the range [0.05–0.2].

4. The expansion ($0 \leq z/D \leq 1.5$)

Just after the nozzle, the flow has the distinctive characteristics of a jet. It expands with an angle of about 10° and entrains the surrounding fluid. The turbulence kinetic energy is maximum where the mean velocity gradient is maximum (figure 9, $z = 0.4D$). A potential core, in which the turbulence properties are directly related to the inlet conditions, exists up to $z = 0.5D$ (figure 2). At $z = 1.3D$ (figure 9), the turbulence maximum has moved onto the axis. The z -evolution of the flow structure is considerably faster than for a free jet. In a closed-end tube, the lateral confinement prevents the pressure from being uniform in both the axial and radial directions.

5. The transition ($1.5 \leq z/D \leq 4.4$)

At the location where the cross-section area of the jet occupies nearly half of this tube ($z = 1.5D$), the effect of the lateral confinement becomes significant. Farther away, the lateral expansion stops and there exists a core of near constant radius in

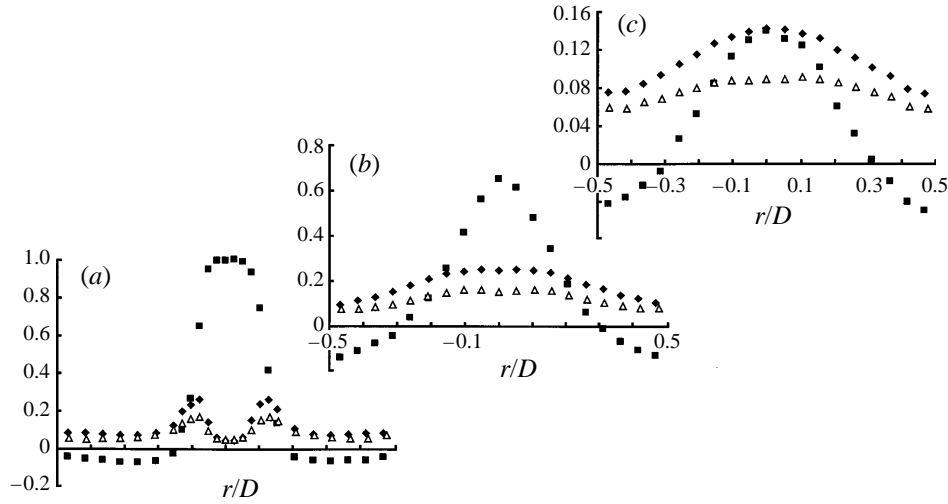


FIGURE 9. Mean and r.m.s. velocities: \blacksquare , U_z/U_0 ; \blacklozenge , $\overline{u_z^2}^{1/2}/U_0$; \triangle , $\overline{u_\theta^2}^{1/2}/U_0$. (a) $z = 0.4D$, (b) $1.3D$, (c) $2.7D$ (negative radii correspond to $\theta = 180^\circ$).

which the velocity is positive ($r < 0.35D$). This core is surrounded by an annular layer in which the velocity is negative ($0.35D < r < 0.5D$). At the core boundary ($r \approx 0.35D$), the radial component of the mean velocity U_r is directed towards the wall. Hence, the bulk velocity in the core decreases with z . Owing to the lateral confinement, the mean flow structure has drastically changed with respect to the region of expansion. Nevertheless, the turbulence is still dominated by similar mechanisms involving production, advection and dissipation (figure 6). In this region, the production of turbulence by the mean velocity gradient and the advection by the mean flow remain constant in comparison with $\overline{u_z^2}^{3/2}/D$. Moreover, the turbulence energy budget shows that the production of turbulence energy is twice the amount that comes from advection. Because the production still dominates in this region, the isotropy ratio $(\overline{u_z^2}/\overline{u_r^2})^{1/2}$ remains greater than unity. The region ends when both r.m.s. velocity and mean velocity have nearly the same magnitude on the axis. Figure 9 shows the radial profiles of statistical moments at this location, i.e. at $z = 2.7D$.

As shown in figure 4, the skewness of the axial velocity fluctuations increases regularly from $z = 2D$, indicating that the relative contribution of the turbulent diffusion in the axial direction increases with z . At $z = 3D$, this diffusion becomes predominant in the equation for $\overline{u_z^2}$, its relative importance increasing up to $z = 4D$. Thus, the axial component of the velocity fluctuations is mainly controlled by the diffusion and dissipation processes. For $z \geq 4D$, the diffusion still dominates although its contribution gradually diminishes to the same order as advection by the mean flow. The radial component of the velocity fluctuations is qualitatively governed by the same mechanism, but the contribution of the turbulent diffusion is less substantial.

As the turbulence production decreases with z , the Reynolds stress tensor becomes less anisotropic. Indeed figure 3 shows that $(\overline{u_z^2}/\overline{u_r^2})^{1/2}$ drops in the range $3D \leq z \leq z_e$. However, the return to isotropy is expected to be faster for the smaller scales, as illustrated through the power spectra of the axial and the lateral velocity fluctuations on the axis (figure 10). For $z \leq 4D$, isotropy is only satisfied by the smallest eddies corresponding to highest frequencies. As the turbulence production decreases when z increases, isotropy is achieved for eddies of larger scales, so that the u_z - and u_r

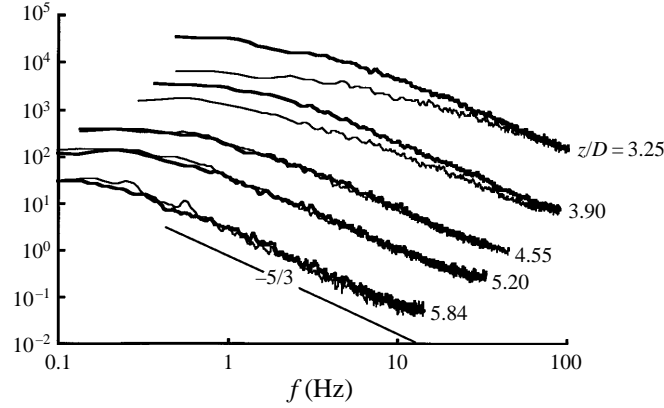


FIGURE 10. Power spectra of u_z and u_r on the axis: —, u_z ; — —, u_r .

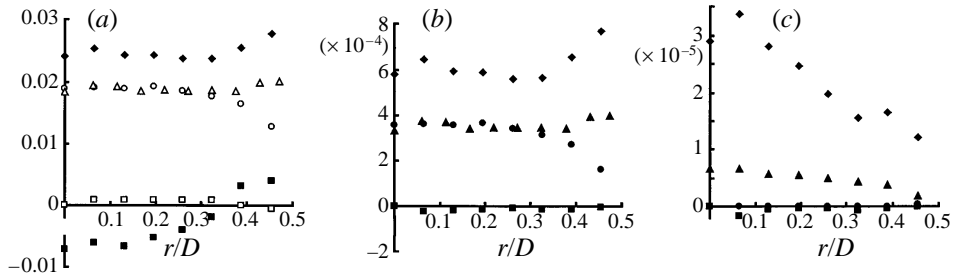


FIGURE 11. Kinematic structure at $z = 3.9D$: (a) ■, U_z/U_0 ; □, U_r/U_0 ; ◆, $\overline{u_z^{1/2}}/U_0$; ○, $\overline{u_r^{1/2}}/U_0$; △, $\overline{u_\theta^{1/2}}/U_0$. (b) ◆, $\overline{u_z^2}/U_0^2$; ●, $\overline{u_r^2}/U_0^2$; ▲, $\overline{u_\theta^2}/U_0^2$; ■, $\overline{u_z u_r}/U_0^2$. (c) ◆, $\overline{u_z^3}/U_0^3$; ●, $\overline{u_r^3}/U_0^3$; ▲, $\overline{u_z u_r^2}/U_0^3$; ■, $\overline{u_z^2 u_r}/U_0^3$.

– spectra become almost indistinguishable for $z \geq z_e$. Since the smallest-scale eddies are isotropic in the whole domain, there is an important consequence. The dissipation rates of u_z^2 and u_r^2 are the same. Therefore, as the diffusion of the axial component is greater than the radial component, the redistribution by pressure fluctuations remains the single candidate for compensating this difference in the budget of $\overline{u_z^2}$ and $\overline{u_r^2}$, (A2) and (A3). The pressure fluctuations are thus responsible for the evolution toward a state of energetic isotropy.

Now, let us discuss the consequences on the lateral structure. Figure 11 shows the radial profiles of mean velocities, the r.m.s. velocities and the second- and third-order moments, for $z = 3.9D$. The profile of the axial component of the mean velocity has a minimum (negative value) at the axis and a maximum close to the wall, whereas the radial component is nearly equal to zero. The r.m.s. values of the fluctuating velocities have been plotted for comparison. They are clearly greater than the mean velocity over the whole cross-section, indicating that the turbulence dominates. The components of the Reynolds stress tensor are two-dimensionally isotropic and two-dimensionally homogeneous in a core situated between the axis and $r = 0.35D$. Furthermore, the shear stress $\overline{u_z u_r}$ is negligible compared to the diagonal terms. Yet, the r.m.s. axial fluctuating velocity is 1.3 times greater than the radial one. Here, we are close to the expected equilibrium between turbulence diffusion, dissipation and possibly redistribution by pressure, equation (4).

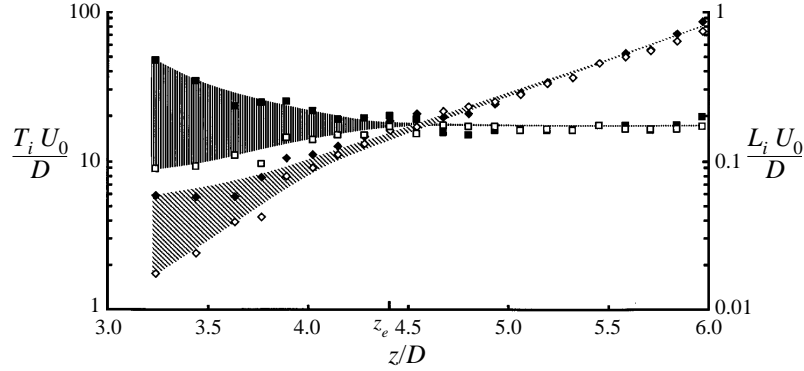


FIGURE 12. Evolution at the axis of integral time scales: \blacklozenge , $T_z U_0/D$; \diamond , $T_r U_0/D$ and length scales obtained from one-point measurements: \blacksquare , L_z/D ; \square , L_r/D .

From $z = 4D$, the turbulent diffusion in the axial direction decreases quickly whereas the energy tends to isotropy which is reached at z_e . Before studying the final region, we will discuss the behaviour of the time and length scales in the transition region. The Eulerian integral time scales T_z and T_r were obtained from integration of the autocorrelation functions:

$$T_z = \int_0^{\infty} R_{zz}(\tau) d\tau \quad \text{and} \quad T_r = \int_0^{\infty} R_{rr}(\tau) d\tau. \quad (6)$$

T_z and T_r are plotted in dimensionless form in figure 12. Like the velocity scales, these time scales tend to an asymptotic exponential behaviour which is nearly reached at $z = 3.9D$. However, in the transition region, T_z is always greater than T_r . Another physical feature can be elucidated from the evolution of the characteristic length scales L_z and L_r , which can be formed by the products of the time scales and the r.m.s. velocities: $L_z = T_z(u_z^2)^{1/2}$, $L_r = T_r(u_r^2)^{1/2}$. These scales are plotted in the same figure in dimensionless form. In the transition region, L_z is greater than L_r and the difference between them decreases when z increases. This gives the rough impression that the largest eddies are flattened in the radial direction in the transition region. Finally, L_z and L_r both tend towards the same constant value of about $0.16D$. This asymptotic value is reached by L_r at $z = 3.9D$; whereas it is reached by L_z at the greater distance from the inlet of z_e . This consolidates what has been pointed out in figure 5 about the velocity scales. For the second-order, like the fourth-order, moments, the lateral components reach asymptotic equilibrium before the axial ones. It seems that the mechanism leading to isotropy makes the energy of the axial fluctuations tend to the level of the radial ones.

As defined above, the length scales L_z and L_r are determined from one-point measurements. Their interpretation is not simple because they are not representative of the real spatial structure of the turbulence field. In order to determine the integral length scales, Λ , two-point measurements are needed since, in the absence of mean motion, such scales cannot be deduced from the Eulerian integral time scales. From these measurements, the spatial cross-correlation coefficients,

$$f(\Delta z) = \frac{\overline{u_z(z,0)u_z(z+\Delta z,0)}}{[\overline{u_z^2(z,0)} \overline{u_z^2(z+\Delta z,0)}]^{1/2}}, \quad g(\Delta r) = \frac{\overline{u_z(z,0)u_z(z,\Delta r)}}{[\overline{u_z^2(z,0)} \overline{u_z^2(z,\Delta r)}]^{1/2}}, \quad (7)$$

were determined first. The corresponding results at $z/D = 3.9, 4.5$ and 5.2 are plotted

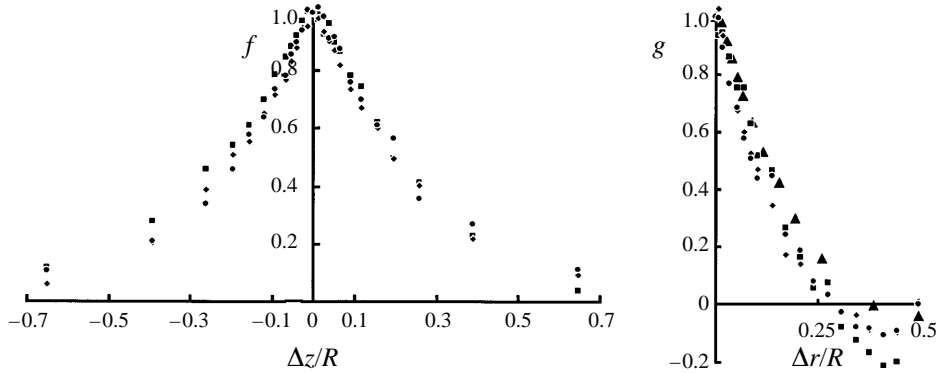


FIGURE 13. Longitudinal and lateral cross-correlations, $f(\Delta z)$ and $g(\Delta r)$ at: \blacksquare , $z = 3.9D$; \blacklozenge , $z = 4.5D$; \bullet , $z = 5.2D$; \blacktriangle , g from equation (8).

z/D	3.9	4.5	5.2
A_{zz}^-/D	0.30	0.25	0.26
A_{zz}^+/D	0.26	0.27	0.29
A_{zz}^-/D	0.28	0.26	0.28
A_{zr}/D	0.096	0.095	0.099

TABLE 2. Integral length scales

in figure 13. Neither $f(\Delta z)$ nor $g(\Delta r)$ depend significantly upon the distance to the nozzle. Although the turbulence is not homogeneous, $f(\Delta z)$ is almost symmetrical. For isotropic homogeneous turbulence, the relation between longitudinal and lateral correlations (Batchelor 1953, p. 46) is

$$g = f + \frac{1}{2}rf'. \quad (8)$$

To verify this, the value of g , calculated using (8) from experimental values of f , is shown in figure 13. Theoretical and experimental values of function g coincide for short separations, but for large separations, the lateral confinement causes a faster decay than in unbounded homogeneous turbulence. The velocities at two points further apart than $D/2$ are still significantly correlated. The corresponding length scales have been evaluated by integration of these curves:

$$A_{zz}^- = \int_{-\infty}^0 f(\zeta) d\zeta, \quad A_{zz}^+ = \int_0^{+\infty} f(\zeta) d\zeta, \quad A_{zz} = \frac{1}{2}(A_{zz}^- + A_{zz}^+), \quad A_{zr} = \int_0^{D/2} g(\rho) d\rho. \quad (9)$$

The results are presented in table 2. It is seen that the two integral scales remain constant, their values being $A_{zz} = 0.28D \pm 7\%$ and $A_{zr} = 0.097D \pm 3\%$. The longitudinal integral length scale is close to the value $A_{zz} = 0.27D$ obtained in turbulent channel by Comte-Bellot (1965). The lateral one is close to the value $A = 0.07D$ determined by Khoo *et al.* (1992) from PIV measurements. In isotropic homogeneous turbulence, integration of (8) shows that the longitudinal scale is twice the lateral one. Here, due to lateral confinement which forces the fluctuations to cancel at the wall, we found the larger value $A_{zz}/A_{zr} = 2.9$. In diffusive turbulence generated by an oscillating grid, the integral length scales are known to increase

linearly with the distance from the grid. This is also the case in grid turbulence in which the size of the largest eddies increases with the distance. In contrast, the size of the largest turbulent eddies grows to the size of the tube. This is achieved at $z = 3.9$. Then, the lateral confinement restricts the size of the largest eddies which stop enlarging.

Let us briefly summarize the role of the transition region in which the flow restructures from a typical shear flow to a flow dominated by turbulent diffusion. Two sub-transitions are observed. The first takes place at the location where the mean flow interacts with the tube boundary. The jet expansion is stopped, then the mean velocity gradually decreases and the flow starts to be dominated by the turbulence. The second transition appears when the natural tendency for the largest eddies to increase their size is stopped by the lateral confinement. From these observations it can be inferred that the role of the lateral confinement is two-fold. On the one hand, it forces the mean flow to vanish, leaving the main role to the fluctuating motion. On the other hand, it maintains the size of the largest eddies of this fluctuating motion constant. The turbulence which emerges from the transition region possesses some peculiarities which should be emphasized. It is dominated by diffusion and the size of its largest eddies is restricted. This turbulence will be further referred to as 'confined diffusive turbulence', in contrast to the classical 'free diffusive turbulence' obtained in grid experiments in unbounded domains.

6. The self-preserving confined diffusive turbulence ($z/D > 4.4$)

Although the integral length scales and the lateral r.m.s. velocities reach their asymptotic behaviour at $z = 3.9D$, the other moments only do so at $z = z_e$. Energetic isotropy is achieved. The major consequence is that any ratio involving two moments remains constant since these moments follow the same law of decay (5). The numerical values of some of these ratios have been determined at the tube axis and are presented in table 3. They have been obtained either from averaging 17 values of the moments distributed in the range $z_e < z < 6.0D$ (the r.m.s. is then indicated) or from least-squares fitting of the exponential curve. The result is remarkable: these ratios are very simple rational numbers. The mean velocity U_z of the residual flow is half the r.m.s. of each component. The third-order moment of the axial component $\overline{u_z^3}$ is equal to the cube of the r.m.s. velocity and to twice the third-order cross-moment $u_z \overline{u_r^2}$. The results obtained by Hanoun *et al.* (1988) in their experiment on turbulence behind an oscillating grid present the same feature. They found that $\overline{u_z \bar{e}} = 2\overline{u_z^3}$, a result which holds in the present experiment also. This specific outcome suggests generalizing to higher-order moments the simple behaviours which were found for the second-, third- or fourth-order moments. For example, the isotropy of the second-order moments is also satisfied at the fourth order. We have tried checking this property for the even moments of higher order and although they seem to follow the expected tendency, the poor accuracy in calculating these moments does not allow any firm conclusions. Another example is the generalization of the relation which holds for the third-order moment $\overline{u_z^3} = \overline{u_z^2}^{3/2}$. It seems that the odd moments of order $2n + 1$ of the axial component are equal to the corresponding even moments of order $2n$ to the power $2n/(2n + 1)$. It may be noted in passing that this power is a necessary condition for the relation to be consistent from the dimensional point of view. The existence of recurrence relationships for any order moments is conceivable, and knowledge of this would make possible a complete description of the statistical properties of the

	$\frac{(\overline{u_r^2})^{1/2}}{(\overline{u_z^2})^{1/2}}$	$\frac{U_z}{(\overline{u_z^2})^{1/2}}$	$\frac{(\overline{u_z^3})^{1/3}}{(\overline{u_z^2})^{1/2}}$	$\frac{\overline{u_z u_r^2}}{\overline{u_z^3}}$	$\frac{\overline{u_r^4}}{\overline{u_z^2}}$	$\frac{\overline{u_r^4}}{\overline{u_z^4}}$
Mean value (ensemble average)	1.014	-0.463	1.001	0.465	6.293	0.931
$\frac{\text{r.m.s. value}}{\text{mean value}}$ (ensemble average)	0.026	0.124	0.041	0.249	0.153	0.133
Mean value (after smoothing)	1.00	-0.48	0.95	0.52	5.98	1.10

TABLE 3. Ratio of statistical moments in the self-preserving zone

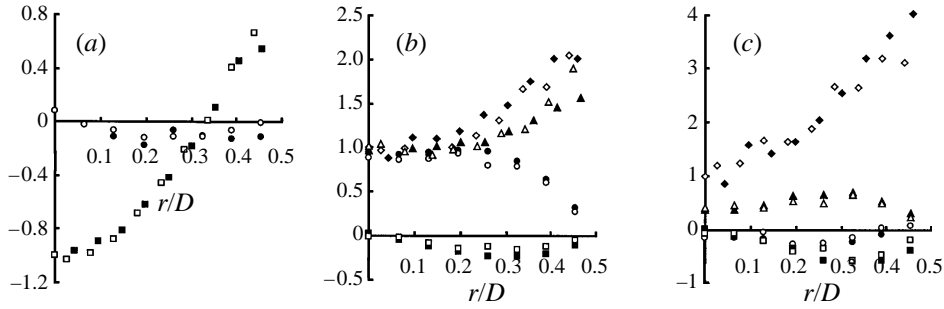


FIGURE 14. Self-preserving property at two different locations (solid symbols refer to $z = 4.5D$, and open symbols to $z = 5.2D$): (a) $\blacksquare, \square, U_z/|U_z|_{r=0}; \bullet, \circ, U_r/|U_z|_{r=0}$. (b) $\blacklozenge, \circ, \overline{u_z^2}/\overline{u_z^2}_{r=0}; \bullet, \circ, \overline{u_r^2}/\overline{u_z^2}_{r=0}; \blacktriangle, \triangle, \overline{u_\theta^2}/\overline{u_z^2}_{r=0}; \blacksquare, \square, \overline{u_z u_r}/\overline{u_z^2}_{r=0}$. (c) $\blacklozenge, \circ, \overline{u_z^3}/\overline{u_z^3}_{r=0}; \bullet, \circ, \overline{u_r^3}/\overline{u_z^3}_{r=0}; \blacktriangle, \triangle, \overline{u_z u_r^2}/\overline{u_z^3}_{r=0}; \blacksquare, \square, \overline{u_z u_r}/\overline{u_z^3}_{r=0}$.

turbulence in the strongly non-Gaussian case. However, we did not succeed in finding such recurrence rules from theoretical considerations.

Another interesting property of the region of exponential decay is the self-similarity of the kinematic profiles. In order to illustrate this result, the radial profiles of the moments up to the third order are plotted in figure 14. The various moments are normalized by the axis values of U_z for the mean velocity components, of $\overline{u_z^2}$ for the second-order moments and of $\overline{u_z^3}$ for the third-order moments. The radial profile of each quantity at a distance z_2 is identical to the profile at z_1 multiplied by the exponential decay between z_2 and z_1 . Thus, in taking into account (5), any moment of order n can be expressed in the form

$$M_n(r, z) = M_n(0, z_0)F(r) \exp\left[-n\frac{z - z_0}{L}\right], \quad (10)$$

where F is a function that depends only on r . As a consequence, all the terms in (A1) decay as $\exp[-3(z - z_0)/L]$ except for the molecular diffusion $\mathcal{D}\nu$ which decreases as $\exp[-2(z - z_0)/L]$. Here, the molecular diffusion of velocity fluctuations is negligible, but for large enough z , the law of decay shows that it should become dominant. As in grid turbulence experiments, the last stage of decay would be driven by viscous effects. The viscous-to-turbulent diffusion ratio is given by $1.5 \times 10^{-6} \exp(-z/L)$. In the present experiment, this ratio is thus equal to 0.003 at the end of the tube, i.e. for $z = 7.7D$.

Let us come back to figure 14 to point out that the components of the Reynolds stress tensor are isotropic and two-dimensionally homogeneous in a central core of radius $r \leq 0.2D$. Near the tube wall, the radial velocity fluctuations are reduced, although the axial and azimuthal fluctuations are increased. The velocity power

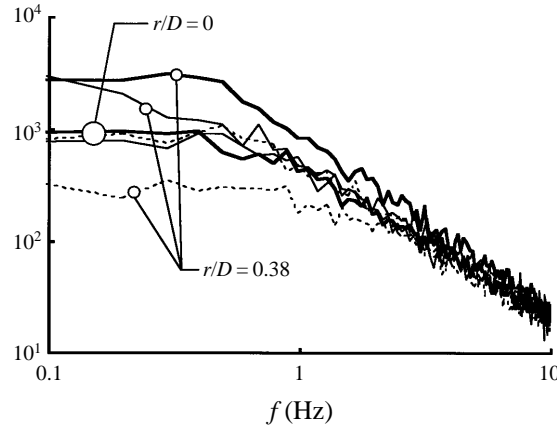


FIGURE 15. Velocity power spectra at $z = 5.2D$: —, u_z ; ---, u_r ; — · —, u_θ .

spectra of figure 15 show that this anisotropy is clearly visible for the smallest frequencies, i.e. for the largest eddies, whereas the energy density of the fluctuating velocity components coincides for high frequencies in both radial locations $r = 0$ and $r = 0.38D$. This anisotropy of the largest eddies is again a consequence of the flow confinement. Radial fluctuations are mainly caused by eddies with azimuthal or axial vorticity. These eddies cannot induce radial fluctuations at a distance from the wall smaller than their radius. It must be also pointed out that the domain of homogeneity is less extended than at $z = 3.9D$. This is due to the alterations of the profiles of $\overline{u_z^2}$ and $\overline{u_\theta^2}$, whereas the profile of $\overline{u_r^2}$ remains the same. Not only is the exponential decay of the radial velocity fluctuations reached, but also its self-similarity is achieved before that of the other components. Concerning the triple correlations, it may be seen (figure 14) that the relative magnitude of the moments corresponding to the radial turbulent diffusion is greater than for $z = 3.9D$, although it remains significantly smaller than the magnitude of the moments corresponding to axial diffusion. Nevertheless, the comparison of radial and axial length scales suggests that r -derivatives are larger than z -derivatives. Therefore, the relative importance of radial and axial diffusion may be clearly established only by exploring the different terms of (A1).

As mentioned before, the law of decay of the various moments of turbulence is a direct consequence of flow confinement. The length scale of the largest eddies is restricted. Let us consider a self-similar diffusive turbulence. Following our definition, any two terms of the energy budget have a constant ratio. In such a case, the flux of energy in the z -direction must necessarily be proportional to $\overline{\partial u_z^3}/\partial z$, whatever the nature of the transport. This energy is supplied through the energy cascade to the turbulent dissipation which can be taken proportional to $-\overline{u_z^3}/A_{zz}$. It yields

$$\frac{\partial \overline{u_z^3}}{\partial z} = -C \frac{\overline{u_z^3}}{A_{zz}}, \quad (11)$$

where C is a dimensionless constant. If A_{zz} increases linearly, the z -decay follows a power law, while if A_{zz} remains constant the decay is exponential with respect to z . It must be stressed that neither a zero mean flow assumption nor isotropy and homogeneity are required to reach this conclusion.

It should be pointed out that similar simple situations are used as reference cases

for the determination of the parameters of turbulent models. Sonin (1983) used results of decaying grid turbulence experiments to establish a relation between the constants σ_k , σ_ϵ , C_μ , C_ϵ , $C_{\epsilon 2}$ of the $k - \epsilon$ model (for definitions, see Rodi 1980). Assuming one-dimensional diffusive turbulence and kinetic turbulent energy decaying in z^{-n} , he found

$$\sigma_k/\sigma_\epsilon = \frac{3n^2 C_{\epsilon 2}}{2(1+2n)(1+3n/2)}. \quad (12)$$

However, if we consider an exponential decay we find

$$\sigma_k/\sigma_\epsilon = \frac{1}{2} C_{\epsilon 2}. \quad (13)$$

Lele (1985) considered the diffusion in a quiescent fluid of turbulence produced by a planar source. He established a relation of consistency

$$\sigma_k/\sigma_\epsilon = 6((4C_{\epsilon 2}^2 + 1)^{1/2} - 2C_{\epsilon 2}). \quad (14)$$

Although these relations are all based upon ideal situations of diffusive turbulence, they are all different. Furthermore, they are generally not satisfied by the usual sets of constants. Following Rodi (1980), if we take $\sigma_k = 1$, $\sigma_\epsilon = 1.3$, $C_{\epsilon 2} = 1.92$, (12) implies a decay exponent of $n = 4.9$ instead of the $n = 2$ found experimentally. Therefore, two-equation one-point closure models are not able to predict such flows, dominated by turbulent transport.

7. Turbulence budgets in the region dominated by diffusion

Additional insight can be gained from the analysis of the energy budgets of the axial and radial velocity fluctuations in the region dominated by turbulent diffusion. First, they will be presented and discussed in the transition region at $z = 3.9D$. Then, we shall consider the self-similar region.

7.1. The transition region

Figure 16 shows the radial profiles of the terms governing the equations for $\overline{u_z^2}$ and $\overline{u_r^2}$ (A2) and (A3), for $z = 3.9D$. The non-starred quantities are defined in the appendix, the stars denote that these quantities are normalized by the value of $\overline{u_z^2}^{3/2}/D$ on the axis. Neither dissipation nor terms involving pressure fluctuations have been measured. In each equation, they are grouped in the rest which is defined as $\mathcal{R}est_i = \mathcal{T}p_i + \mathcal{R}p_i + \mathcal{E}_i$. Neither was the correlation between u_r and u_θ measured. As a consequence, the turbulent diffusion $\mathcal{T}u_{rr}$ presented here is incomplete. Thus, the remaining term of the $\overline{u_r^2}$ equation also contains the correlation $2\overline{u_r u_\theta^2}/r$ which is responsible for energy transfer between radial and azimuthal components of the velocity fluctuations. Although this correlation vanishes at the axis, it may become significant far from it. Besides, in the region under consideration the flow has not yet reached its asymptotic behaviour. The determination of the z -derivatives of the moments involved in some of the terms ($\mathcal{A}d_{zz}$, $\mathcal{A}d_{rz}$, $\mathcal{P}r_{zz}$, $\mathcal{P}r_{rz}$, $\mathcal{T}u_{zz}$ and $\mathcal{T}u_{rz}$) would require the measurement of the z -evolution of these moments at different r -locations. We have thus used a simplification assuming that their relative decay is the same as at the axis. For each moment $M_n(z, r)$, this assumption reads

$$\frac{\partial M_n}{\partial z} \approx \frac{M_n}{(M_n)_{r=0}} \left(\frac{\partial M_n}{\partial z} \right)_{r=0}. \quad (15)$$

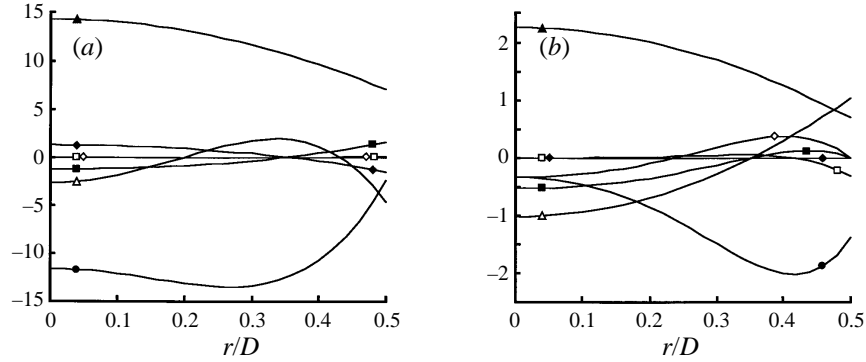


FIGURE 16. Normal Reynolds stresses budget at $z = 3.9D$. (a) z -component: \blacksquare , Ad_{zz}^* ; \square , Ad_{zr}^* ; \blacklozenge , $\mathcal{P}i_{zz}^*$; \diamond , $\mathcal{P}i_{zr}^*$; \blacktriangle , $\mathcal{T}u_{zz}^*$; \triangle , $\mathcal{T}u_{zr}^*$; \bullet , $Rest_z^*$. (b) r -component: \blacksquare , Ad_{rz}^* ; \square , Ad_{rr}^* ; \blacklozenge , $\mathcal{P}i_{rz}^*$; \diamond , $\mathcal{P}i_{rr}^*$; \blacktriangle , $\mathcal{T}u_{rz}^*$; \triangle , $\mathcal{T}u_{rr}^*$; \bullet , $Rest_r^*$.

The profiles presented in figure 16 are, thus, exact on the axis, but only approximate far from it.

The advection of energy by the radial mean flow is negligible in both the $\overline{u_z^2}$ and $\overline{u_r^2}$ equations, $Ad_{zr} \approx 0$ and $Ad_{rr} \approx 0$. The same conclusion holds for the production terms $\mathcal{P}i_{zr}$ and $\mathcal{P}i_{rz}$ since the turbulent shear stress $-\rho\overline{u_z u_r}$ is weak. In addition, the advection by the axial mean flow (Ad_{zz} , Ad_{rz}) and the production by normal turbulent stress ($\mathcal{P}i_{zz}$, $\mathcal{P}i_{rr}$) are significantly smaller than the axial turbulent diffusion ($\mathcal{T}u_{zz}$, $\mathcal{T}u_{rz}$). Nevertheless, the radial turbulent diffusions ($\mathcal{T}u_{zr}$, $\mathcal{T}u_{rr}$) due to the velocity fluctuations u_r are not negligible in spite of the homogeneity of the Reynolds stress tensor near the axis. While the contribution of $\mathcal{T}u_{zr}$ remains very weak in the equation for $\overline{u_z^2}$, $\mathcal{T}u_{rr}$ is significant in the equation for $\overline{u_r^2}$.

Figure 17 summarises the energy transfers for a certain volume of fluid located at the axis. The left- and right-hand boxes contain the energy in the axial and radial velocity fluctuations respectively. The arrows joining the boxes represent the energy transfer between the two velocity components while the others represent the spatial flux in the given direction. The corresponding value of the dimensionless energy transfer is given on each arrow. The energy of the z -velocity component is mainly supplied by the axial turbulent diffusion since the corresponding term is dominant ($\mathcal{T}u_{zz}^* = 14.4$). The same is true for the energy of the r -component ($\mathcal{T}u_{rz}^* = 2.3$). The radial turbulent diffusion also plays a role, but not to the same extent, in the energy budget ($\mathcal{T}u_{zr}^* = 2.7$ and $\mathcal{T}u_{rr}^* = 1.0$). With regard to these values, the turbulent fluxes with respect to z supply more energy to the z - than to the r -fluctuating component, acting against the turbulence isotropy. It may be noted in passing that the production through normal stresses also opposes the return to isotropy ($\mathcal{P}i_{zz}^* = 1.3$ and $\mathcal{P}i_{rr}^* = \mathcal{P}i_{\theta\theta}^* = -0.35$). Indeed, it induces an energy transfer from the mean flow and from the radial and azimuthal velocity fluctuations to the axial component of the turbulence.

At this location, the turbulence behaviour is close to the ideal case of diffusive turbulence that we have defined in the introduction. The turbulence energy of the axial fluctuations mainly results from the axial diffusion–dissipation balance. Concerning the energy budget of the radial fluctuations, the radial turbulent diffusion has also to be taken into account. As a whole, the diffusion mechanism of the turbulent kinetic energy seems to be that described by (4). As the axial diffusion of the z -velocity fluctuations is much greater than for the r -velocity, the evolution of

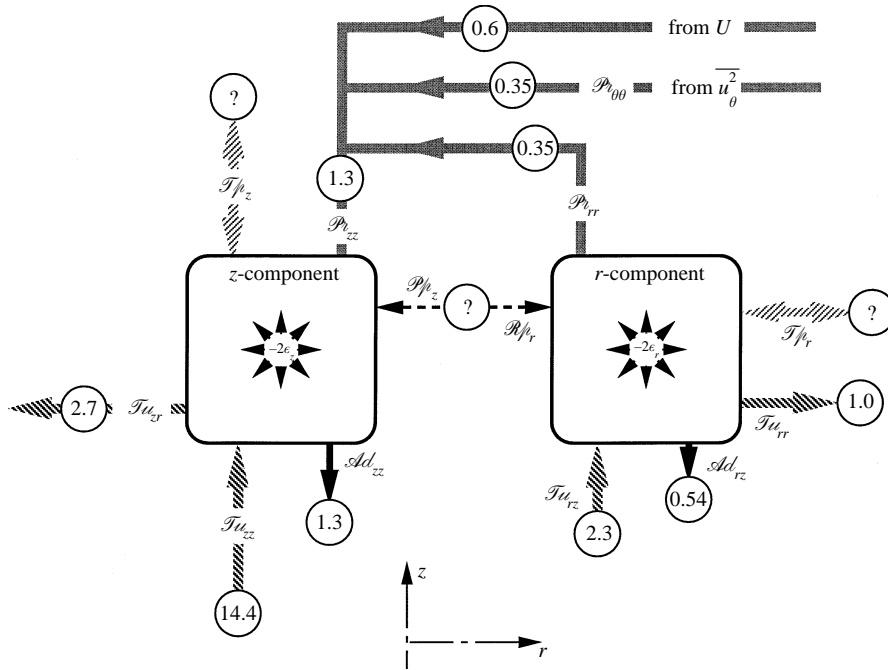


FIGURE 17. Energy transfer on the axis at $z = 3.9D$ ($\overline{u_z^2} = 1.7\overline{u_r^2}$).

the turbulent stress tensor toward isotropy is necessarily due to the terms involving pressure fluctuations. However, this energetic isotropy has not yet been reached for $z = 3.9D$, since the ratio between z - and r -velocity fluctuations is still 1.3. This value is nearly the same as the values that have been obtained in oscillating grid experiments, for example Hannoun *et al.* (1988) found 1.32.

7.2. The self-preserving region

From z_e , all the statistical moments reach their asymptotic state and the turbulence structure is self-preserving. Figure 18 shows the radial profiles of the terms governing the equations for $\overline{u_z^2}$ and $\overline{u_r^2}$, (A2) and (A3), at any cross-section of the final zone. This figure is similar to figure 16, and the same remarks concerning $\mathcal{R}est_i$ apply. Nevertheless, an important difference must be pointed out: owing to the decaying property of the various moments, (15) is exact so that no approximation is needed to determine the z -derivatives away from the axis.

The structure of the turbulence field, shown in figure 18, has changed considerably compared to the results of figure 16. Energetic isotropy is reached, but the flow remains homogeneous in a central core limited to $r \leq 0.2D$. In the energy budget, only the advection by the radial mean flow (Ad_{zr}, Ad_{rr}) and the turbulence production by turbulent shear stress ($\mathcal{P}_{v_{zr}}, \mathcal{P}_{v_{rz}}$) remain negligible. The relative contributions of both advection by the axial mean flow (Ad_{zz}, Ad_{rz}) and production by normal stresses ($\mathcal{P}_{v_{zz}}, \mathcal{P}_{v_{rr}}$) are greater than in the transition region. The major contributions are still those of turbulence diffusion although axial diffusion ($\mathcal{T}u_{zz}, \mathcal{T}u_{rz}$) is smaller here than in the transition region and than radial diffusion ($\mathcal{T}u_{zr}, \mathcal{T}u_{rr}$).

To understand the role of each contribution, the energy budget on the axis is plotted in figure 19. Let us consider, as a first step, the transfers of energy in the axial

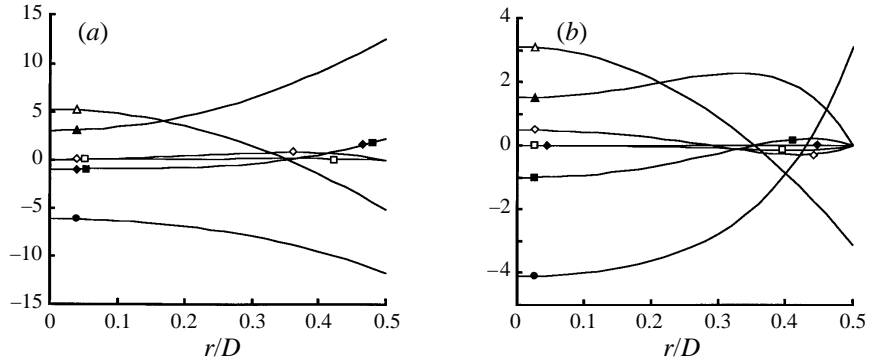


FIGURE 18. Normal Reynolds stresses budget in the self-preserving zone. (a) z-component: \blacksquare , Ad_{zz}^* ; \square , Ad_{zr}^* ; \blacklozenge , $\mathcal{P}i_{zz}^*$; \diamond , $\mathcal{P}i_{zr}^*$; \blacktriangle , $\mathcal{T}u_{zz}^*$; \triangle , $\mathcal{T}u_{zr}^*$; \bullet , Res_{zz}^* . (b) r-component: \blacksquare , Ad_{rz}^* ; \square , Ad_{rr}^* ; \blacklozenge , $\mathcal{P}i_{rz}^*$; \diamond , $\mathcal{P}i_{rr}^*$; \blacktriangle , $\mathcal{T}u_{rz}^*$; \triangle , $\mathcal{T}u_{rr}^*$; \bullet , Res_{rr}^* .

direction. As in figure 17, the turbulent diffusion of the z-component is greater than for the r-component since $\mathcal{T}u_{zz}^* = 3$ and $\mathcal{T}u_{rz}^* = 1.5$. This difference is still against the isotropy of the Reynolds stress tensor. In contrast to this, the advection by the axial mean velocity is the same for the two velocity components ($Ad_{zz}^* = Ad_{rz}^* = -1$). The residual mean flow has another effect through the production by turbulent normal stress ($\mathcal{P}i_{zz}^*$ and $\mathcal{P}i_{rr}^*$). In isotropic situations, the sum of these terms exactly vanishes in the turbulent kinetic energy balance, because of mass conservation. Then, the role of $\mathcal{P}i_{zz}^*$ and $\mathcal{P}i_{rr}^*$ consists in transferring the energy between the turbulent velocity components. Here, the energy is taken from axial velocity fluctuations ($\mathcal{P}i_{zz}^* = -1$) and given to lateral velocity fluctuations ($\mathcal{P}i_{rr}^* = \mathcal{P}i_{\theta\theta}^* = +0.5$). Interestingly, the difference $\mathcal{P}i_{zz}^* - \mathcal{P}i_{rr}^*$ compensates the difference of axial diffusion:

$$\mathcal{T}u_{zz}^* + Ad_{zz}^* + \mathcal{P}i_{zz}^* = \mathcal{T}u_{rz}^* + Ad_{rz}^* + \mathcal{P}i_{rr}^* = 1. \quad (16)$$

Thus, the difference between the axial diffusion of $\overline{u_z^2}$ and $\overline{u_r^2}$ is compensated independently of the terms involving the pressure fluctuations. It must be stressed that this mechanism of energy transfer acts in such a way that it consolidates the isotropy only if the mean velocity gradient $\partial U_z / \partial z$ is positive. This is the case here but not at $z = 3.9D$. For this velocity gradient to contribute to the return to isotropy, the mean velocity U_z must be negative since it must go to zero at infinity. Thus, it may be stated that the isotropy of energy is related to a negative axial velocity ($U_z < 0$). Another argument in favour of this assumption is that the energetic isotropy is obtained at the cross-section, z_e , where the sign of the velocity gradient changes (figure 2).

As a second step, let us discuss the transfer of energy in the radial direction (figure 19). Even if the gradients of the second-order moments are small in a large region around the axis, the radial turbulent diffusion is dominant ($\mathcal{T}u_{zr}^* = 5.2$, $\mathcal{T}u_{rr}^* = 3.1$). It must be noted that the turbulent diffusion is non-zero even with zero gradient ($\partial \overline{u_z^2} / \partial r \approx 0$, $\partial \overline{u_r^2} / \partial r \approx 0$). In contrast to what is observed in the axial direction, u_r is better correlated with u_z^2 than with u_r^2 . Consequently, the radial diffusion of the axial component is more effective than that of the radial one. Besides, as suggested by the velocity power spectra, the dissipation is the same for axial and radial fluctuations ($\epsilon_z = \epsilon_r$). This remark leads to an interesting consequence for the energy balance. Equation (16) may be written by replacing each side by its expression taken from

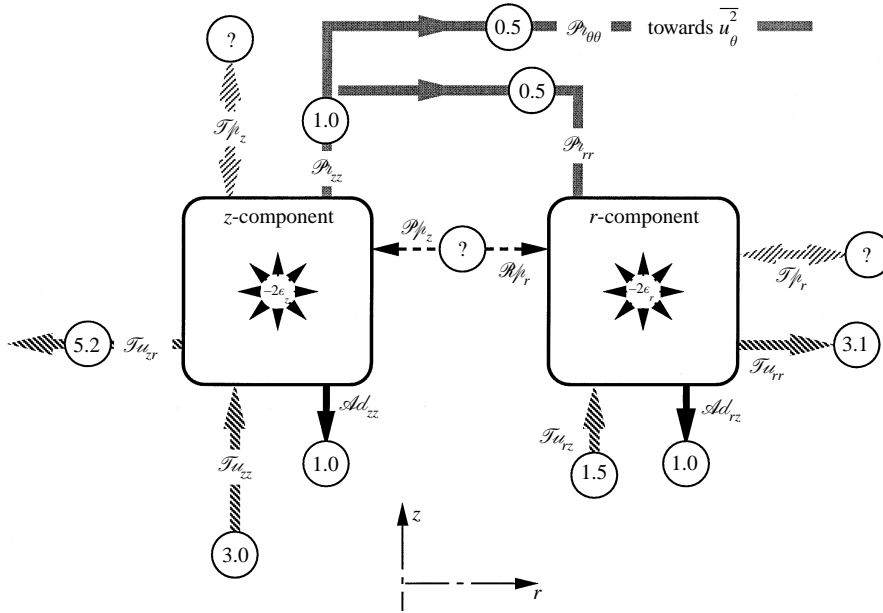


FIGURE 19. Energy transfer on the axis in the self-preserving zone ($\overline{u_z^2} = \overline{u_r^2}$).

(A2) and (A3) respectively. On discarding the negligible terms, this yields

$$\mathcal{T}u_{zr}^* + \mathcal{R}\rho_z^* + \mathcal{T}\rho_z^* = \mathcal{T}u_{rr}^* + \mathcal{R}\rho_r^* + \mathcal{T}\rho_r^*. \tag{17}$$

Thus the difference between the radial turbulent diffusions of z - and r -components ($\mathcal{T}u_{zr}^* = 5.2$, $\mathcal{T}u_{rr}^* = 3.1$) must be compensated by the terms involving the pressure fluctuations ($\mathcal{T}\rho_z^*$, $\mathcal{R}\rho_z^*$, $\mathcal{T}\rho_r^*$, $\mathcal{R}\rho_r^*$) for isotropy to be maintained away from the axis.

The physical mechanisms that control the self-preserving diffusive region appear to be very different from the ideal ones, discussed in the introduction. Let us recall the main features of the flow structure. The isotropy and homogeneity of the Reynolds stress tensor are accurately obtained in a core region extending over about half the tube width. The mean motion remains smaller than the turbulent motion since the axial mean velocity is half of its r.m.s. fluctuation. Even if the mean motion is essential for the diffusion balance, its kinetic energy represents only 1/12 of this of turbulence. Thus, from energy considerations, i.e. for the second moments, the core region can be said to be isotropic, two-dimensionally homogeneous and free of mean flow. However, this conclusion does not hold for the third-order moments. Those corresponding to axial diffusion are not zero on the axis, but they remain constant in the core region. In contrast, those corresponding to radial diffusion vanish at the axis but increase with r . Depending on the direction under consideration, the mechanisms are entirely different. In the axial direction, the structure is non-homogeneous, but the energetic isotropy is realized and maintained. Besides, the imbalance between axial and radial diffusion is compensated by a redistribution mechanism due to the presence of a positive gradient of mean velocity. In the radial direction homogeneity and isotropy are realized at the second order. The diffusion imbalance has to be compensated by the terms involving pressure fluctuations. It must be stressed that there exists a turbulent transport in the absence of a Reynolds stress gradient.

In the absence of radial homogeneity, no reason permits *a priori* the expectation

of independence between axial and radial transfers. Besides, the terms \mathcal{T}/ρ_z , which is related to axial transport by fluctuating pressure in (17), remains.

8. Discussion and conclusions

The theoretical issue, addressed in the introduction, can be summarized by the following question. Does a stationary turbulent field without mean motion or two-dimensionally homogeneous and energetically isotropic exist? Such a turbulent field is the archetype of ‘diffusive turbulence’, that is a turbulence dominated by turbulent diffusion and dissipation. The first motivation for tackling this problem is the design of an experimental tool for studying the specific role of the turbulence upon other phenomena. The second is to improve our knowledge of turbulent transport mechanisms.

First, the work presented here is an attempt to experimentally generate a flow field as close as possible to the ideal situation. Our method consists of using a jet – a classical turbulent shear flow that is strongly inhomogeneous – in a confined geometry. The results obtained here show that the flow field actually reaches a state essentially dominated by the turbulent diffusion, but this situation is much more complicated than the ideal case. As expected, the combination of longitudinal and lateral confinement causes the mean flow to decrease progressively with z to zero. After a distance from the inlet $z/D = 3$, the turbulence is essentially controlled by a balance between turbulent transport and dissipation. Up to $z/D = 4$, the flow field is very close to the one obtained in oscillating grid experiments and the large scales of turbulence increase. However, near $z/D = 4$, the size of the largest eddies reaches the tube diameter and stops growing. The tube boundaries act as a spatial filter upon the eddy sizes. Hence, the lateral confinement restructures the flow again. It reaches the asymptotic state of ‘confined diffusive turbulence’, near $z_c = 4.4D$. The properties of this turbulence have been determined in the present work. They are summarized as follows: the integral scales remain constant; in the central part of the tube ($r/D \leq 0.2$), the Reynolds stress tensor is quite isotropic and two-dimensionally homogeneous; all the statistical moments follow the same exponential law of decay, leading to a self-preserving flow; a secondary mean flow exists whose energy is about 1/12 the turbulent kinetic energy.

Now, let us compare this particular turbulence with that obtained in oscillating grid facilities. Though the way of generating turbulence is very different, the disparities between the two kinds of experiments are, in fact, due to the size of the vessel. Indeed, in oscillating grid experiments the lateral dimension is large in comparison with the size of the largest eddies. Thus, the asymptotic state obtained can be called ‘free diffusive turbulence’. The integral length scales increase linearly with the distance from the grid. Is this situation nearer the ideal case than confined diffusive turbulence? Concerning isotropy, the answer is no. Fernando & De Silva (1993) have summarized the results of oscillating grid experiments and the ratio between longitudinal and lateral r.m.s. velocities is about 1.2. For the presence of secondary mean flow, the answer is less clear. As already mentioned, large mean flow structures have been observed by Hopfinger & Toly (1976) and McDougall (1979) in oscillating grid experiments, but Fernando & De Silva (1993) have shown that they can be suppressed by a judicious choice of the grid shape. Still, there is no evidence that a weak mean flow related to turbulence mechanisms does not exist as in confined jet experiments, but how weak is weak? Following Hopfinger & Toly (1976), weak

means that the kinetic energy of the mean flow is about 10% of the turbulent kinetic energy which is similar to the level that we found.

There is at present no experimental evidence that energetically isotropic and two-dimensionally homogeneous turbulence does exist in the absence of mean flow. Why is this so? It is generally considered that the cause of anisotropy is turbulence production. It is expected that, in the absence of production, isotropy could be realized. Although true for homogeneous turbulence, this conclusion has to be reconsidered for diffusive turbulence. Indeed, the lack of homogeneity in one direction is another cause of anisotropy through the triple correlations. On the one hand, their existence violates the necessary condition of isotropy. On the other hand, they lead to a difference of diffusion between longitudinal and lateral fluctuations that has to be compensated. In the present confined jet experiment, an original mechanism involving the mean velocity gradient of the secondary flow compensates this imbalance. In oscillating grid experiments, only the pressure fluctuations can redistribute the excess of diffusion of the longitudinal fluctuations over the lateral ones; however, all experimental results show that the Reynolds stress tensor is not isotropic.

Despite this result, diffusive turbulence remains a very interesting tool for studying the role of turbulence in specific problems. For this purpose, researchers can now use two types of experimental system: the oscillating grid and the confined jet in a closed tube. The first generates unbounded turbulence with kinetic energy decreasing as the square of the distance from the grid and integral length scales increasing linearly. The second produces confined diffusive turbulence with turbulent kinetic energy decaying exponentially with the distance from the nozzle and integral length scales remaining constant. In both systems, the turbulent kinetic energy can be varied without modifying the flow structure; it is at least one order of magnitude greater than that of mean flow.

In general, turbulent flows dominated by triple correlations are poorly understood. Up to now, three different situations have been investigated by several authors. The first and simplest case corresponds to 'free diffusive turbulence' in which neither advection nor a boundary are present (see the introduction for references). The second is 'confined diffusive turbulence', discussed in the present article, in which the boundaries play a significant role. The third is the shearless turbulence mixing layer of Veeravalli & Warhaft (1989), in which the flow is controlled by turbulent transport in the spanwise direction and by advection in the streamwise direction. For these different cases, the statistics of the velocity field are non-Gaussian and the flow is highly intermittent. Veeravalli & Warhaft and the present results have shown that if the statistics are Gaussian in the regions where the flow is dominated by production and/or advection, they are not where turbulent transport is predominant.

Another property, exhibited in these two situations, is that turbulent transport cannot be fully explained by a diffusion mechanism. To explain the spreading mechanism of their mixing layer, Veeravalli & Warhaft have distinguished 'turbulent diffusion' from the mixing by 'intermittent penetration'. Likewise, we have shown here that significant turbulent transport takes place in the radial direction although Reynolds stress gradients are negligible. Thus, if only one-point moments are considered, third-order moments are needed to take into account the influence of the confinement. The consequences are of major importance for modelling. For instance, it is not surprising that the different attempts of Sonin (1983) and Lele (1985) to use diffusive turbulence for adjusting the constants of $k-\epsilon$ models lead to contradictory results: the triple correlations or the turbulent transport by pressure cannot always be expressed as functions of the Reynolds stresses.

Appendix A. Notation and equations

The equations for the turbulent energy are written below in Cartesian and cylindrical coordinates for steady flow. U_i and u_i denote the i -components of the mean and fluctuating velocities, p the fluctuating pressure. The overbar is used to denote the time averages of the correlations. With the intention of emphasizing the role of each term of the balance equations for the Reynolds stresses, these terms are designated as $\mathcal{A}d$ for the advection by the mean flow, $\mathcal{T}\rho$ and $\mathcal{T}u$ for the turbulent transport (also called turbulent diffusion) by pressure and velocity fluctuations, $\mathcal{R}\rho$ for the redistribution by pressure fluctuations, $\mathcal{P}i$ for the production, $\mathcal{D}v$ for the diffusion by viscosity and \mathcal{E} for the dissipation by turbulent motion. In the figures and the discussion these quantities are denoted by a star when they are normalized by the axis value of u_z^{*2}/D .

A.1. Normal Reynolds stress equations in Cartesian coordinates

Let $e = u_x^2 + u_y^2 + u_z^2$ be the instantaneous energy of the turbulent motion. Its time average \bar{e} involves the contribution \bar{u}_i^2 of each component i of the fluctuating velocity. The balance equation for each contribution may be written

$$\mathcal{A}d_i + \mathcal{T}\rho_i + \mathcal{R}\rho_i + \mathcal{P}i + \mathcal{T}u_i + \mathcal{D}v_i + \mathcal{E}_i = 0, \quad (\text{A } 1)$$

with the following definitions:

$$\begin{aligned} \mathcal{A}d_i &= - \left(U_x \frac{\partial}{\partial x} + U_y \frac{\partial}{\partial y} + U_z \frac{\partial}{\partial z} \right) \bar{u}_i^2, \quad \mathcal{T}\rho_i = - \frac{2}{\rho} \frac{\partial}{\partial x_i} \overline{p u_i}, \quad \mathcal{R}\rho_i = \frac{2}{\rho} \overline{\frac{\partial u_i}{\partial x_i}}, \\ \mathcal{P}i &= -2 \left(\overline{u_i u_x} \frac{\partial}{\partial x} + \overline{u_i u_y} \frac{\partial}{\partial y} + \overline{u_i u_z} \frac{\partial}{\partial z} \right) U_i, \quad \mathcal{T}u_i = - \left(\frac{\partial}{\partial x} \overline{u_x u_i^2} + \frac{\partial}{\partial y} \overline{u_y u_i^2} + \frac{\partial}{\partial z} \overline{u_z u_i^2} \right) \\ \mathcal{D}v_i &= \nu \nabla^2 \bar{u}_i^2, \quad \mathcal{E}_i = 2\epsilon_i = -2\nu \left[\left(\frac{\partial u_i}{\partial x} \right)^2 + \left(\frac{\partial u_i}{\partial y} \right)^2 + \left(\frac{\partial u_i}{\partial z} \right)^2 \right]. \end{aligned}$$

With these definitions, each term corresponding to a gain of energy is positive.

A.2. Normal Reynolds stress equations in cylindrical coordinates

The above equations are written below for an axisymmetric flow. The diffusion by viscosity $\mathcal{D}v$ being negligible, it will thus be disregarded. The fluxes by pressure (velocity) fluctuations $\mathcal{T}\rho$ ($\mathcal{T}u_i$) will be split into their axial and radial contributions $\mathcal{T}\rho_{iz}$ and $\mathcal{T}\rho_{ir}$ ($\mathcal{T}u_{iz}$ and $\mathcal{T}u_{ir}$). In a like manner, $\mathcal{P}i$ will be split into the production by normal and shear stresses. The equation for \bar{u}_z^2 becomes

$$\mathcal{A}d_{zz} + \mathcal{A}d_{zr} + \mathcal{T}\rho_z + \mathcal{R}\rho_z + \mathcal{P}i_{zz} + \mathcal{P}i_{zr} + \mathcal{T}u_{zz} + \mathcal{T}u_{zr} + \mathcal{E}_z = 0, \quad (\text{A } 2)$$

with the following definitions:

$$\begin{aligned} \mathcal{A}d_{zz} &= -U_z \frac{\partial}{\partial z} \bar{u}_z^2, \quad \mathcal{A}d_{zr} = -U_r \frac{\partial}{\partial r} \bar{u}_z^2, \quad \mathcal{T}\rho_z = - \frac{2}{\rho} \frac{\partial}{\partial z} \overline{p u_z}, \quad \mathcal{R}\rho_z = \frac{2}{\rho} \overline{p \frac{\partial u_z}{\partial z}}, \\ \mathcal{P}i_{zz} &= -2 \bar{u}_z^2 \frac{\partial U_z}{\partial z}, \quad \mathcal{P}i_{zr} = -2 \bar{u}_z u_r \frac{\partial U_z}{\partial r}, \quad \mathcal{T}u_{zz} = - \frac{\partial}{\partial z} \overline{u_z^3}, \quad \mathcal{T}u_{zr} = - \frac{1}{r} \frac{\partial}{\partial r} \overline{r u_r u_z^2}, \\ \mathcal{E}_z &= 2\epsilon_z = -2\nu \left[\left(\frac{\partial u_z}{\partial z} \right)^2 + \left(\frac{\partial u_z}{\partial r} \right)^2 + \left(\frac{1}{r} \frac{\partial u_z}{\partial \theta} \right)^2 \right]. \end{aligned}$$

The equation for $\overline{u_r^2}$ reads

$$\mathcal{A}d_{rz} + \mathcal{A}d_{rr} + \mathcal{T}\overline{u_r} + \mathcal{R}\overline{u_r} + \mathcal{P}\overline{u_{rz}} + \mathcal{P}\overline{u_{rr}} + \mathcal{T}u_{rz} + \mathcal{T}u_{rr} + \mathcal{E}_r = 0, \quad (\text{A } 3)$$

with

$$\begin{aligned} \mathcal{A}d_{rz} &= -U_z \frac{\partial \overline{u_r^2}}{\partial z}, & \mathcal{A}d_{rr} &= -U_r \frac{\partial \overline{u_r^2}}{\partial r}, & \mathcal{T}\overline{u_r} &= -\frac{2}{\rho} \frac{\partial}{\partial r} \overline{p u_r}, & \mathcal{R}\overline{u_r} &= \frac{2}{\rho} \overline{p} \frac{\partial \overline{u_r}}{\partial r}, \\ \mathcal{P}\overline{u_{rz}} &= -2\overline{u_z u_r} \frac{\partial U_r}{\partial z}, & \mathcal{P}\overline{u_{rr}} &= -2\overline{u_r^2} \frac{\partial U_r}{\partial r}, & \mathcal{T}u_{rz} &= -\frac{\partial}{\partial z} \overline{u_z u_r^2}, \\ \mathcal{T}u_{rr} &= -\frac{\partial}{\partial r} \overline{u_r^3} + \frac{2}{r} \overline{u_r u_\theta^2}, & \mathcal{E}_r &= 2\epsilon_r = -2\nu \left[\left(\frac{\partial \overline{u_r}}{\partial z} \right)^2 + \left(\frac{\partial \overline{u_r}}{\partial r} \right)^2 + \left(\frac{1}{r} \frac{\partial \overline{u_r}}{\partial \theta} \right)^2 \right]. \end{aligned}$$

The equation for $\overline{u_\theta^2}$ will not be written: only the term $\mathcal{P}\overline{u_{\theta\theta}}$ needs to be expressed. It is similar to $\mathcal{P}\overline{u_{zz}}$ and $\mathcal{P}\overline{u_{rr}}$ for the azimuthal fluctuations, $\mathcal{P}\overline{u_{\theta\theta}} = -2U_r \overline{u_\theta^2}/r$. On the axis of symmetry it is equal to $\mathcal{P}\overline{u_{rr}}$.

REFERENCES

- BATCHELOR, G. K. 1953 *The Theory of Homogeneous Turbulence*. Cambridge University Press.
- BATCHELOR, G. K. & TOWNSEND, A. A. 1947 Decay of isotropic turbulence in the initial period. *Proc. R. Soc. Lond. A* **193**, 539.
- BOUVARD, M. & DUMAS, H. 1967 Application de la mesure du fil chaud à la mesure de la turbulence dans l'eau. *Houille Blanche* **22**, 257–278, 723–733.
- BROWN, J. S., KHOO, B.-C. & SONIN, A. A. 1990 Rate correlation for condensation of pure vapor on turbulent, subcooled liquid. *Intl J. Heat Mass Transfer*, **33**, 2001–2018.
- BRUMLEY, B. H. & JIRKA, G. H. 1987 Near-surface turbulence in a grid-stirred tank *J. Fluid Mech.* **183**, 235–263.
- CHASSAING, P. 1979 Mélange turbulent de gaz inertes dans un jet de tube libre. Thèse de doctorat d'état, Institut National Polytechnique de Toulouse.
- COMTE-BELLOT, G. 1965 Ecoulements turbulents entre deux parois parallèles. Service de Documentation Scientifique et Technique de l'Armement Edition.
- COMTE-BELLOT, G. & CORRISIN, S. 1971 Simple Eulerian time correlation of full- and narrow-band velocity signals in grid-generated, 'isotropic' turbulence. *J. Fluid Mech.* **48**, 273–337.
- CORRISIN, S. 1963 *Encyclopedia of Physics*, vol. 8, part 2, p. 568. Springer.
- DE SILVA, I. P. D. & FERNANDO, H. J. S. 1992 Some aspects of mixing in a stratified turbulent patch. *J. Fluid Mech.* **240**, 601–625.
- FERNANDO, H. J. S. & DE SILVA, I. P. D. 1993 Note on secondary flows in oscillating-grid, mixing box experiments. *Phys. Fluids A* **5**, 1849–1851.
- HANNOUN, I. A., FERNANDO, H. J. S. & LIST, E. J. 1988 Turbulence structure near a sharp density interface. *J. Fluid Mech.* **189**, 189–431.
- HOPFINGER, E. J. & TOLY, J. A. 1976 Spatially decaying turbulence and its relation to mixing across density interface. *J. Fluid Mech.* **78**, 155–175.
- KHOO, B.-C., CHEW, T. C., HENG, P. S. & KONG, H. K. 1992 Turbulence characterisation of a confined using PIV. *Exps. Fluids* **13**, 350–356.
- KHOO, B.-C. & SONIN, A. A. 1992 Scalar rate correlation at a turbulent liquid free surface: a two-regime correlation for high Schmidt numbers. *Intl J. Heat Mass Transfer* **35**, 2223–2244.
- LELE, K. S. 1985 A consistency condition for Reynolds stress closures. *Phys. Fluids* **28**, 64–68.
- MCDUGALL, T. J. 1979 Measurements of turbulence in a zero-mean-shear mixed layer. *J. Fluid Mech.* **94**, 409–431.
- MAGNAUDET, J. 1993 Modelling of inhomogeneous turbulence in the absence of mean velocity gradients. *Appl. Sci. Res.* **51**, 525–531.
- RODI W. 1980 Turbulence models and their applications in hydraulic. A state of the art paper. *IAHR (sec. on fund. of division II), Exp. and Math. Fluids Dynamics*.
- ROSENBERG, 1963 Abramovich, G. N. *The Theory of Turbulent Jets*. M.I.T. Press.

- ROUSE, H. & DODU, J. 1955 Diffusion turbulente à travers une discontinuité de densité *Houille Blanche* **10**, 522–532.
- RISSE, F. 1994 Déformation et rupture d'une bulle dans une turbulence diffusive. Thesis, INP Toulouse, France.
- SONIN, A. A. 1983 Calibration of the k - ϵ turbulence model for the diffusion of turbulence. *Phys. Fluids* **26**, 2769.
- SONIN, A. A., SHIMKO, M. A. & CHUN, J.-H. 1986 Vapor condensation onto a turbulent liquid – I. The steady condensation rate as a function of liquid-side turbulence. *Intl J. Heat Mass Transfer* **29**, 1319–1332.
- STEWART, R. W. & TOWNSEND, A. A. 1951 Similarity and self-preservation in isotropic turbulence. *Phil. Trans. R. Soc. Lond. A* **243**, 359.
- SUNYACH, M. & MATHIEU, J. 1969 Zone de mélange d'un jet plan. Fluctuations induites dans le cône à potentiel-intermittence. *Intl J. Heat Mass Transfer* **12**, 1679–1697.
- THOMPSON, S. M. & TURNER, J. S. 1975 Mixing across an interface due to turbulence generated by an oscillating grid. *J. Fluid Mech.* **67**, 349–368.
- TURNER, J. S. 1968 The influence of molecular diffusivity on turbulent entrainment across a density interface. *J. Fluid Mech.* **33**, 639–656.
- ÜBEROI, M. S. 1963 Energy transfer in isotropic turbulence. *Phys. Fluids* **6**, 1048–1056.
- VEERAVALLI, S. & WARHAFT, Z. 1989 The shearless turbulence mixing layer. *J. Fluid Mech.* **207**, 191–229.